NAVAL POSTGRADUATE SCHOOL

MONTEREY, CALIFORNIA

THESIS

MODELING, SIMULATION, AND EXPERIMENTAL VALIDATION OF AN ENERGY MANAGEMENT SYSTEM ON A TACTICAL MICROGRID BUILT WITH COMMERCIAL OFF-THE-SHELF COMPONENTS

by

Joshua I. Ashley

September 2023

Thesis Advisor: Giovanna Oriti
Co-Advisors: Preetha Thulasiraman
Daniel Reich

THIS PAGE INTENTIONALLY LEFT BLANK

REPORT DOCUMENTATION PAGE			*Form Approved OMB No. 0704-0188*

1. AGENCY USE ONLY *(Leave blank)*	**2. REPORT DATE** September 2023	**3. REPORT TYPE AND DATES COVERED** Master's thesis

4. TITLE AND SUBTITLE MODELING, SIMULATION, AND EXPERIMENTAL VALIDATION OF AN ENERGY MANAGEMENT SYSTEM ON A TACTICAL MICROGRID BUILT WITH COMMERCIAL OFF-THE-SHELF COMPONENTS	**5. FUNDING NUMBERS** REKRP
6. AUTHOR(S) Joshua I. Ashley	
7. PERFORMING ORGANIZATION NAME(S) AND ADDRESS(ES) Naval Postgraduate School Monterey, CA 93943-5000	**8. PERFORMING ORGANIZATION REPORT NUMBER**
9. SPONSORING / MONITORING AGENCY NAME(S) AND ADDRESS(ES) NAVFAC, WNY 1322 Patterson Ave SE, Washington, DC, 20374-5140	**10. SPONSORING / MONITORING AGENCY REPORT NUMBER**

11. SUPPLEMENTARY NOTES The views expressed in this thesis are those of the author and do not reflect the official policy or position of the Department of Defense or the U.S. Government.

12a. DISTRIBUTION / AVAILABILITY STATEMENT Approved for public release. Distribution is unlimited.	**12b. DISTRIBUTION CODE** A

13. ABSTRACT (maximum 200 words)

This thesis develops a physics-based model to aid in the design of microgrids for the Department of Defense. The research conducted falls directly in line with efforts to minimize dependence on the utility grid while providing a secure and reliable power network for military facilities and operations. The model is used to simulate the performance of a microgrid under different load conditions and geographic scenarios. It also presents a methodology for processing historical solar irradiance data to estimate future power contribution from a photovoltaic array for a specific geographical location. The model implements an energy management system that controls the microgrid based on monitored values of the components. The results of the simulation outputs are validated against measurements taken from an experimental, commercial off-the-shelf microgrid. The validated model is a valuable tool for the design of future microgrids.

14. SUBJECT TERMS microgrid, power, energy	**15. NUMBER OF PAGES** 81
	16. PRICE CODE

17. SECURITY CLASSIFICATION OF REPORT Unclassified	**18. SECURITY CLASSIFICATION OF THIS PAGE** Unclassified	**19. SECURITY CLASSIFICATION OF ABSTRACT** Unclassified	**20. LIMITATION OF ABSTRACT** UU

NSN 7540-01-280-5500

Standard Form 298 (Rev. 2-89)
Prescribed by ANSI Std. 239-18

THIS PAGE INTENTIONALLY LEFT BLANK

Approved for public release. Distribution is unlimited.

MODELING, SIMULATION, AND EXPERIMENTAL VALIDATION OF AN ENERGY MANAGEMENT SYSTEM ON A TACTICAL MICROGRID BUILT WITH COMMERCIAL OFF-THE-SHELF COMPONENTS

Joshua I. Ashley
Captain, United States Marine Corps
BS, Virginia Military Institute, 2017

Submitted in partial fulfillment of the
requirements for the degree of

MASTER OF SCIENCE IN ELECTRICAL ENGINEERING

from the

NAVAL POSTGRADUATE SCHOOL
September 2023

Approved by: Giovanna Oriti
Advisor

Preetha Thulasiraman
Co-Advisor

Daniel Reich
Co-Advisor

Douglas J. Fouts
Chair, Department of Electrical and Computer Engineering

THIS PAGE INTENTIONALLY LEFT BLANK

ABSTRACT

This thesis develops a physics-based model to aid in the design of microgrids for the Department of Defense. The research conducted falls directly in line with efforts to minimize dependence on the utility grid while providing a secure and reliable power network for military facilities and operations. The model is used to simulate the performance of a microgrid under different load conditions and geographic scenarios. It also presents a methodology for processing historical solar irradiance data to estimate future power contribution from a photovoltaic array for a specific geographical location. The model implements an energy management system that controls the microgrid based on monitored values of the components. The results of the simulation outputs are validated against measurements taken from an experimental, commercial off-the-shelf microgrid. The validated model is a valuable tool for the design of future microgrids.

THIS PAGE INTENTIONALLY LEFT BLANK

Table of Contents

List of Figures

List of Tables

THIS PAGE INTENTIONALLY LEFT BLANK

List of Acronyms and Abbreviations

AGS	advanced generator start
AC	alternating current
BESS	battery energy storage system
COTS	commercial off the shelf
DOD	Department of Defense
DON	Department of the Navy
DERs	distributed energy resources
DC	direct current
EDG	emergency diesel generator
EMS	energy management system
FOB	forward operating base
GHI	global horizontal irradiance
HQST	High Quality Solar Technology
IEEE	Institute of Electrical and Electronics Engineers
MPPT	maximum point power tracking
NREL	National Renewable Energy Laboratory
NPS	Naval Postgraduate School
PV	photovoltaic
SOC	state of charge
USMC	United States Marine Corps

THIS PAGE INTENTIONALLY LEFT BLANK

Acknowledgments

The work and research behind this thesis would not have been as seamless as it was without the guidance and counsel of Dr. Giovanna Oriti. I am grateful for her attentive enthusiasm to provide her insight into my work. I must also highlight the hours spent by Bob Broadston helping me integrate the generator into the microgrid used for this research. Without his help, the findings in this thesis would not have been as valuable as they are. I have nothing but gratitude for these two individuals and my co-advisors for their hand in shaping this thesis. I would also like to take this space to thank my family and friends, without whom I would not be where I am today.

THIS PAGE INTENTIONALLY LEFT BLANK

CHAPTER 1:
Introduction

The objective of this thesis is to validate a physics-based simulation of microgrid performance based on an experimental microgrid. The ability to simulate an energy system that provides power to consumers allows designers to accurately plan for the resources needed to build such a system. A microgrid is a desirable energy framework in the military because it ties different energy sources together to provide reliable power for military operations.

1.1 Motivation

The motivation behind this research is to develop a physics-based model validated by experimental observation into a design tool for planning energy solutions for military operations. The Department of the Navy (DON) operates in environments in which it must be able to sustain itself for extended periods of time. Future engagements will require units to deploy from ships to expeditionary operating areas with little to no support from supply chains. A critical component required to conduct their operations is energy. Energy may be harnessed from various sources, but regardless of source, a significant part of that energy is converted to electricity for uses ranging from powering command and control centers, sensors, weapon system platforms, water purification, and logistical support. The challenge then becomes developing the means by which the Navy and Marine Corps produce their own reliable electrical power for extended periods of time with minimal reliance on supply chains—specifically the giant burden of transporting fossil fuels. The benefit of self-sufficient energy production in military applications from a security, not to mention economic, standpoint cannot be understated [1]. Microgrid technology may be part of the solution to this challenge due to the incorporation of diverse energy sources and prioritization of renewable energy.

1.2 Research Objectives

The research conducted through the development of this thesis serves to address the following objective: build a physics-based model to simulate the performance of the different

components of a microgrid. This model will be tested against the experimental hardware measurements to compare the accuracy of the simulation. The experimental model used to validate the performance of the simulation will be the Naval Postgraduate School (NPS) microgrid composed of photovoltaic panels, lead-acid batteries, a gasoline generator, an inverter-rectifier, and a programmable load [2]. Because solar irradiance data play a large role in the output power of photovoltaic (PV) arrays, the simulation will reference historical irradiance data for a geographical location to help predict future solar energy.

1.3 Related Work

Early microgrid technology dates back as early as the late 19th century but began gaining traction around the turn of the 21st century in search of increasing reliability on the central grid [3]. As the civilian sector continues to develop microgrids for resilience and reliability of the commercial grid, the military also explores to create its energy independence for both bases and forward deployed environments. In 2012, the Marine Corps Expeditionary Energy Office conducted research into the energy usage of a forward operating base (FOB) in Afghanistan [4]. This study measured energy usage of a deployed unit in an effort to better understand the average energy requirement of a standard unit and how it might be met using hybrid systems in lieu of depending solely on diesel generators.

Studying the works of others on microgrids, including the work conducted on the NPS microgrid, has set the foundation for the work ahead in this thesis. Lindstrom's work characterized the performance of a mobile microgrid in two different modes of operation—islanded and grid-connected [5]. He tested the microgrid against four different load sizes using commercial space heaters to compare the response and document his results. His testing on using the grid-connected mode, however, did not include any autonomous control system to switch the system from islanded to grid mode, only manual engagement of grid support.

In 2020, Fish conducted research in designing and modeling a microgrid using measured data of load profiles in an arctic region to develop a control algorithm to prioritize renewable power over fossil-fuel powered generators [6]. Her computer model sought to predict the behavior of a PV array and a battery bank backed up by an emergency diesel generator (EDG) in order to design the components of a microgrid for a user-specified load requirement. She

also used the NPS microgrid to validate her model, but only observed the response of an applied load to the PV array and battery bank without the generator support. Ultimately she validated her model for the response of the PV array and provided a starting point for research exploring the use of other energy sources to supplement power for greater loads when the PV array alone could not reliably support a requirement.

The works above are the starting point for the research in this thesis. It will fill the gaps of research by mathematically modeling a microgrid incorporating specific hardware and environmental data into a simulation. This work will also reference Institute of Electrical and Electronics Engineers (IEEE) Std 1547-2018, which defines the parameters that interconnected distributed energy resources (DERs) must meet, to validate whether findings are within the governing standards [7]. It is important to adhere to military standards throughout the research and design of system in order to ensure that designed loads for military applications are compatible with the energy system that will be powering them.

1.4 Thesis Organization

The remainder of this thesis is organized as follows. Chapter 2 introduces microgrids and discusses the different types of microgrids and the modes in which they operate. Chapter 3 introduces the physics-based model and implementation in MATLAB Simulink. It then discusses the simulation outputs for several different trials to showcase its performance. In Chapter 4, results of the simulation are compared to the data measurements taken from the NPS microgrid in a trial with similar parameters. Lastly, Chapter 5 discusses concluding results and explores future work in this field of research.

THIS PAGE INTENTIONALLY LEFT BLANK

CHAPTER 2:
Background

This chapter describes the architecture of microgrids, their different modes of operation, and their application within the DON.

2.1 Microgrids

As Varley describes, "Microgrids are electrical grid networks that... provide their own sources of power generation such as EDGs or PV arrays" [8]. These networks link multiple DERs and loads, and can operate connected to or independently from the utility grid. Microgrids take advantage of the use of renewable energy and energy storage to provide reliable power while minimizing reliance on power from the utility grid.

There are three different types of microgrids: alternating current (AC), direct current (DC) and hybrid. The difference between these microgrid architectures is how power is distributed. The two most common microgrid architectures are shown in Figure 2.1.

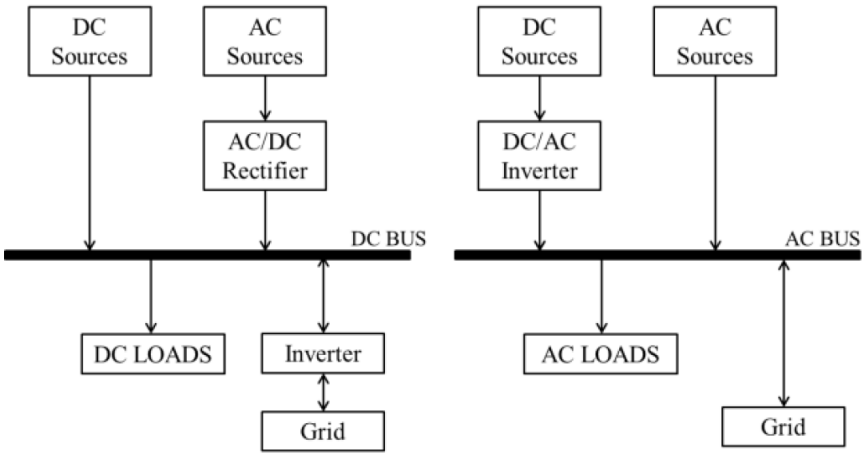

Figure 2.1. Basic DC and AC Microgrid Architecture. Source: [9].

As the name suggests, a DC microgrid has a DC bus to which different DC loads or sources

are connected. Any AC load or source requires a power converter to interface to the bus. DC loads or sources may also require a power conversion stage to regulate the DC voltage. An AC microgrid distributes power via an AC bus. Whereas AC sources and loads are connected directly, DC loads require a rectifier and DC sources require an inverter to interface with the AC bus.

Hybrid microgrids are a combination of these two types to bridge the capability or standardization gap in current infrastructure. An example of a hybrid microgrid is shown in Figure 2.2 and it "consists of [AC] and [DC] networks connected by a bidirectional converter" [10]. Unless a proposed network will incorporate AC or DC components exclusively, a hybrid microgrid offers the greatest versatility for adding components to the network. The experimental portion of this thesis is conducted on a hybrid microgrid.

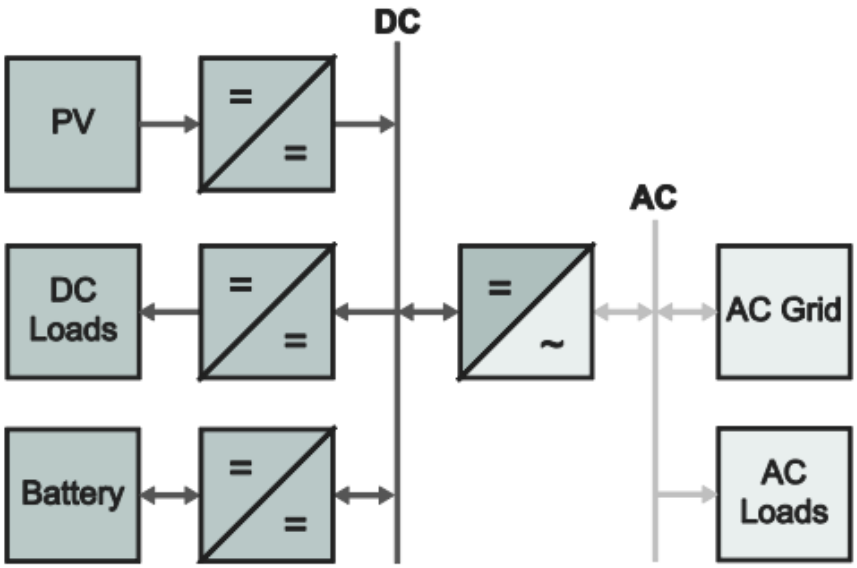

Figure 2.2. Example Hybrid Microgrid Architecture. Source: [10].

Microgrids can also be classified by how they are configured to interact with the utility grid. A microgrid operates in *grid-tied* or *autonomous* (often referred to as *islanded*) modes [11]. A microgrid that is grid-tied is connected to the utility grid and can be mutually supporting. When a microgrid is in islanded mode it is not connected to the utility grid and provides all

of its power internally to its network. The simulation developed in this thesis can easily have the ability to replicated both modes of operation; however, due to the equipment limitations this thesis will focus on operating in the islanded mode.

Another aspect that microgrids have the potential to provide is a layer of security within its power network. Due to its independence from the utility grid, a microgrid can isolate itself from aberrations in the utility grid power resulting from not only environmental disasters but also cyberattacks on infrastructure. This buffer provides a level of security by nature of its inherent architecture.

2.2 Microgrids in the Department of Defense

The importance of microgrids in the DON is highlighted by recent efforts outlined in the Department of the Navy Climate Action 2030. The role microgrids play in these efforts are identified as providing secure energy resilience that also mitigates carbon pollution [12]. Marine Corps Air Station Miramar, CA, is showcased as the exemplary installation incorporating microgrid technology to accomplish the efforts identified in Climate Action 2030. The use of renewable energy sources and microgrid technology cut the installations use of utility grid power nearly in half.

Microgrids serve a purpose not only on permanent installations but also on forward deployed operations. The United States Army showcased this concept in their development of mobile microgrids [13]. Mobile, also referred to as tactical, microgrids can offer the benefit of secure, resilient power that greatly reduces the toll on the logistics of transporting bulk fuel.

Ongoing research and development is leading to wider adoption of microgrid technology in the Department of Defense (DOD). NPS has used its own specifically designed microgrid using commercial off the shelf (COTS) equipment for students to test the implementation of microgrids for military applications [2]. This thesis research uses that microgrid to further the efforts to incorporate this technology for the DOD.

THIS PAGE INTENTIONALLY LEFT BLANK

CHAPTER 3:
Physics-Based Modeling and Simulation

This chapter comprises the microgrid physics-based model description and the simulations of its performance for one or more days of operation under different operating conditions.

3.1 Power Flow Model

To create the physics-based model of a microgrid it is important to be able to describe its operation mathematically. Figure 3.1 highlights the power converter in the microgrid schematic and the assumption that it is an ideal system, where the energy entering the system is equal to the energy leaving the system, neglecting losses and inefficiencies.

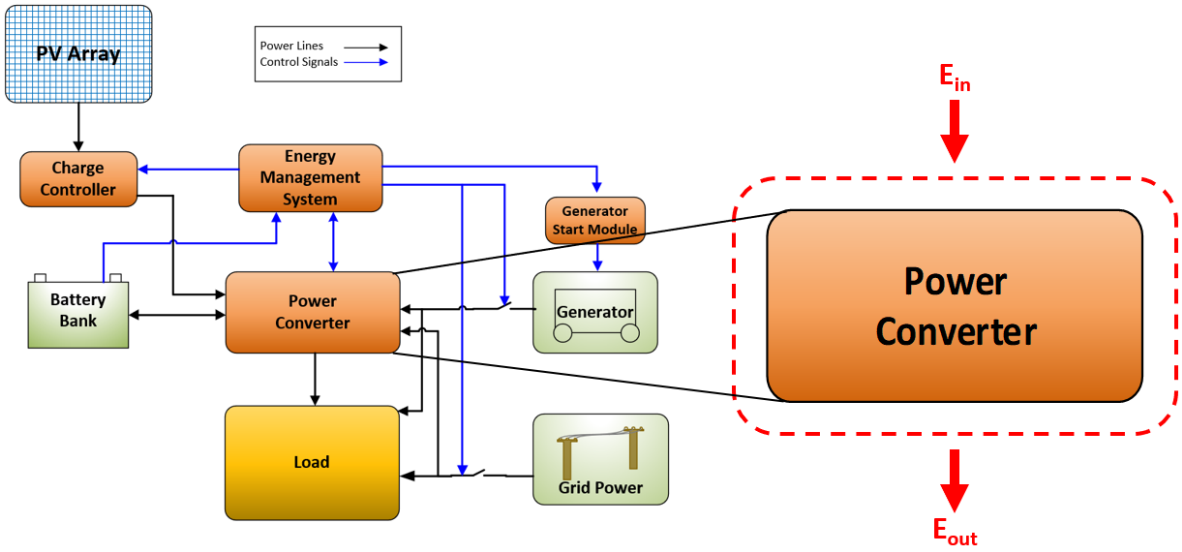

Figure 3.1. Power Flow Model

Because energy in and out is under the same time step, it follows that the power in equals the power out of the system from each energy source. This derivation is shown in (3.1) and (3.2).

$$E_{in} = E_{out} \tag{3.1}$$

$$P_{in} = P_{out} \tag{3.2}$$

$$P_{battery} + P_{PV} + P_{generator} + P_{grid} = P_{load} \tag{3.3}$$

Equation (3.3) governs the operation of the microgrid to model the flow of energy and availability of charge in the battery bank, also referred to as battery energy storage system (BESS). The power converter in Figure 3.2 sums the power from each energy source to equal the power going to the battery according to the following equation:

$$P_{battery} = P_{load} - P_{PV} - P_{generator} - P_{grid} \tag{3.4}$$

Because the experimental model used in this thesis will be operating in islanding mode, the power from the grid is set to zero in Equation 3.4. Simulations for grid-tied microgrids would include a block serving as the utility grid power. Dividing the sum of powers by the battery voltage yields the current flowing in and out of the battery bank including the efficiency of the inverter rectifier. Current into the battery can now be calculated as seen in (3.5) where η_{inv} is the inverter rectifier efficiency and η_{PV} is the solar panel efficiency.

$$I_{battery} = \frac{P_{load} * \eta_{inv} - P_{generator} * \eta_{inv} - P_{PV} * \eta_{PV}}{V_{battery}} \tag{3.5}$$

3.2 Matlab-Simulink Implementation

The model presented in Figure 3.1 was implemented using the Simulink toolbox in MATLAB [14]. The goal of the Simulink model, shown in Figure 3.2, is to simulate the behavior of the microgrid under a specific load with multiple DERs. The simulation operates with a 10-s time step to produce the response of the system over the duration of the trial. The clock drives the look-up tables of data for generator, PV array, and load powers. The 10-s increment matches the measurement intervals for the hardware used in the NPS microgrid.

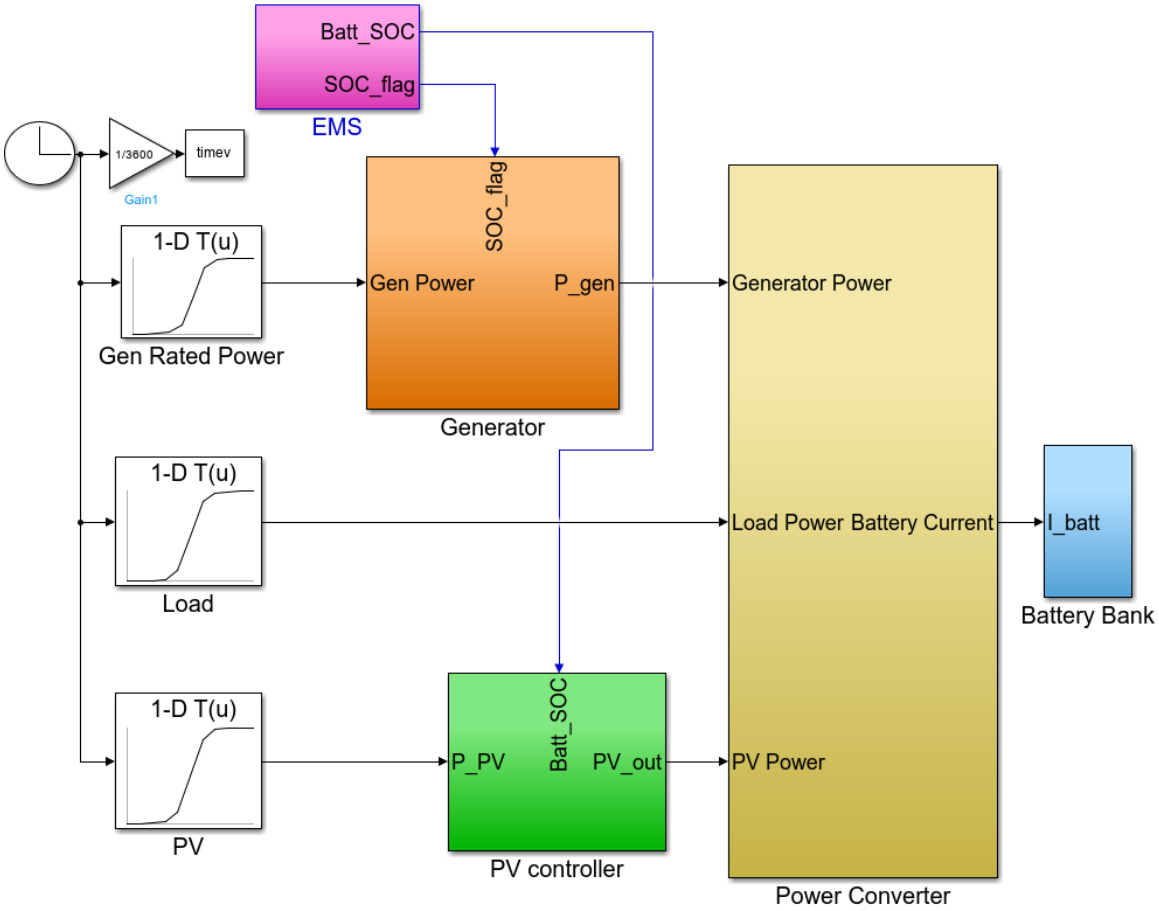

Figure 3.2. Top-Level Simulink Model

3.2.1 Energy Management System

The energy management system (EMS) block in Figure 3.3 functions similar to the hardware feature that monitors state of charge (SOC) of the battery bank and flags the generator to engage or disengage. It uses a relay block and the value of battery SOC from the battery block to generate a logic value that feeds into the generator block to allow generator power to flow through to the power converter. At a value of 60% the logic output is 1 and returns to 0 when SOC reaches 95%. SOC_{flag} runs to the generator to control its output and $Batt_{SOC}$ runs to the PV controller to prevent the power of PV from overcharging the batteries.

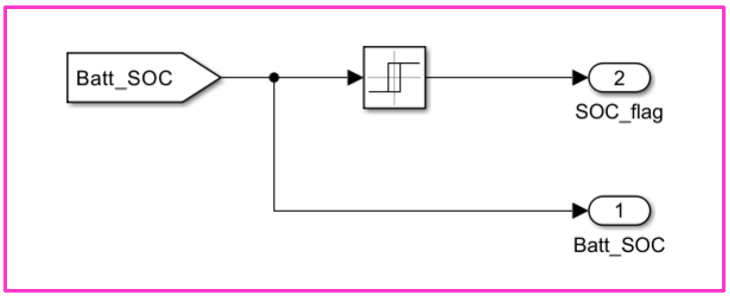

Figure 3.3. Simulink EMS Block

3.2.2 Load Profile

The load look-up table in Figure 3.2 allows the user to input a desired power profile for which the microgrid will provide power. For the initial trials the load profile is kept constant, while for most of the simulated trials a 24-h load profile mimicking a FOB power consumption was used. Measured load profiles can also be used from historical data.

3.2.3 Generator

The generator block in Figure 3.4 receives data corresponding to a constant value which is the rated power for a real generator. The rated power is not the actual power delivered to the system since there are limitations on how much power a generator can supply. One of these limitations is that some generators cannot be operated for sustained periods under a load close to its rated power. Another limitation is the breaker fuses on a generator to prevent drawing excess current from an outlet. To compensate for these limitations, the generator block includes a limiting variable to set the max current produced by the generator.

If the EMS "SOC_{flag}" value is on then the generator will be "turned on" and power will flow to the power converter. Otherwise, the output for the generator is zero. The "Outlet Panel" block at the right of Figure 3.4 contains similar logic that limits the output generator power to a maximum current value. At default, this maximum current value is set to 20 A to match the breaker fuse on the Firman generator in the NPS microgrid for this thesis (later discussed in Section 4.2.4).

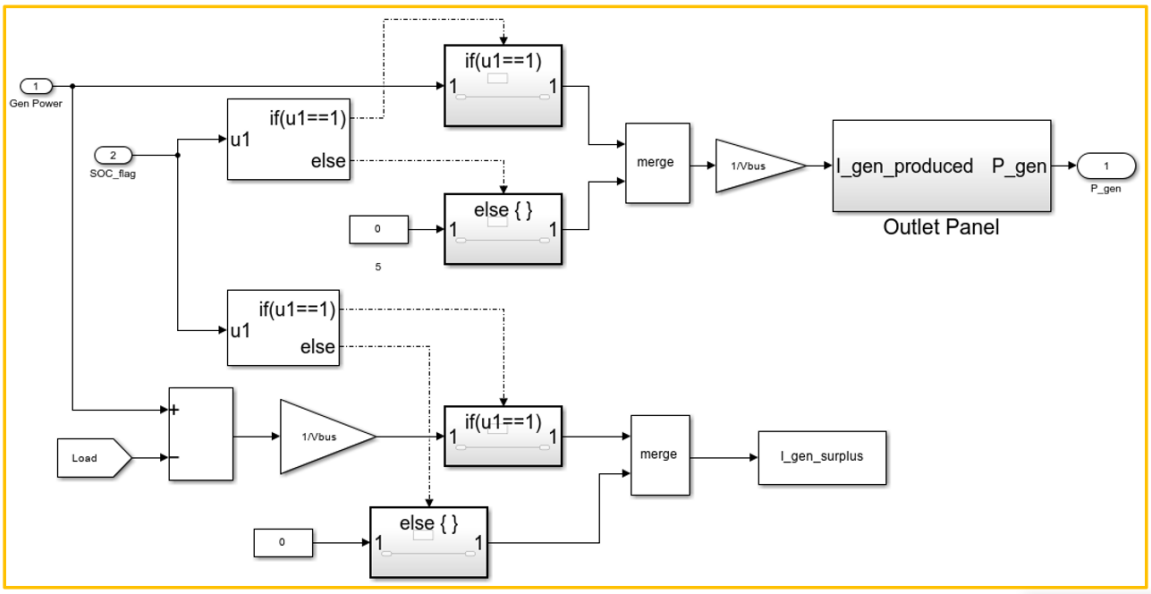

Figure 3.4. Simulink Generator Block

3.2.4 Solar Power

The data entered into the simulation for the input solar energy through the photovoltaic panels is derived from historical solar irradiance data [15]. The National Renewable Energy Laboratory (NREL) hosts an online database for solar radiation based on geographic locations. The radiation data was averaged over a month-long period to derive a predicted solar radiation profile from which the simulation would calculate power received through the PV array.

From the data, the daily measurements for global horizontal irradiance (GHI) and temperature are averaged over a month to determine an expected conditions for a given month in a given geographic area. This data, depicted in Figure 3.5, is used to estimate conditions to determine a predicted power output for a specific type of photovoltaic panel.

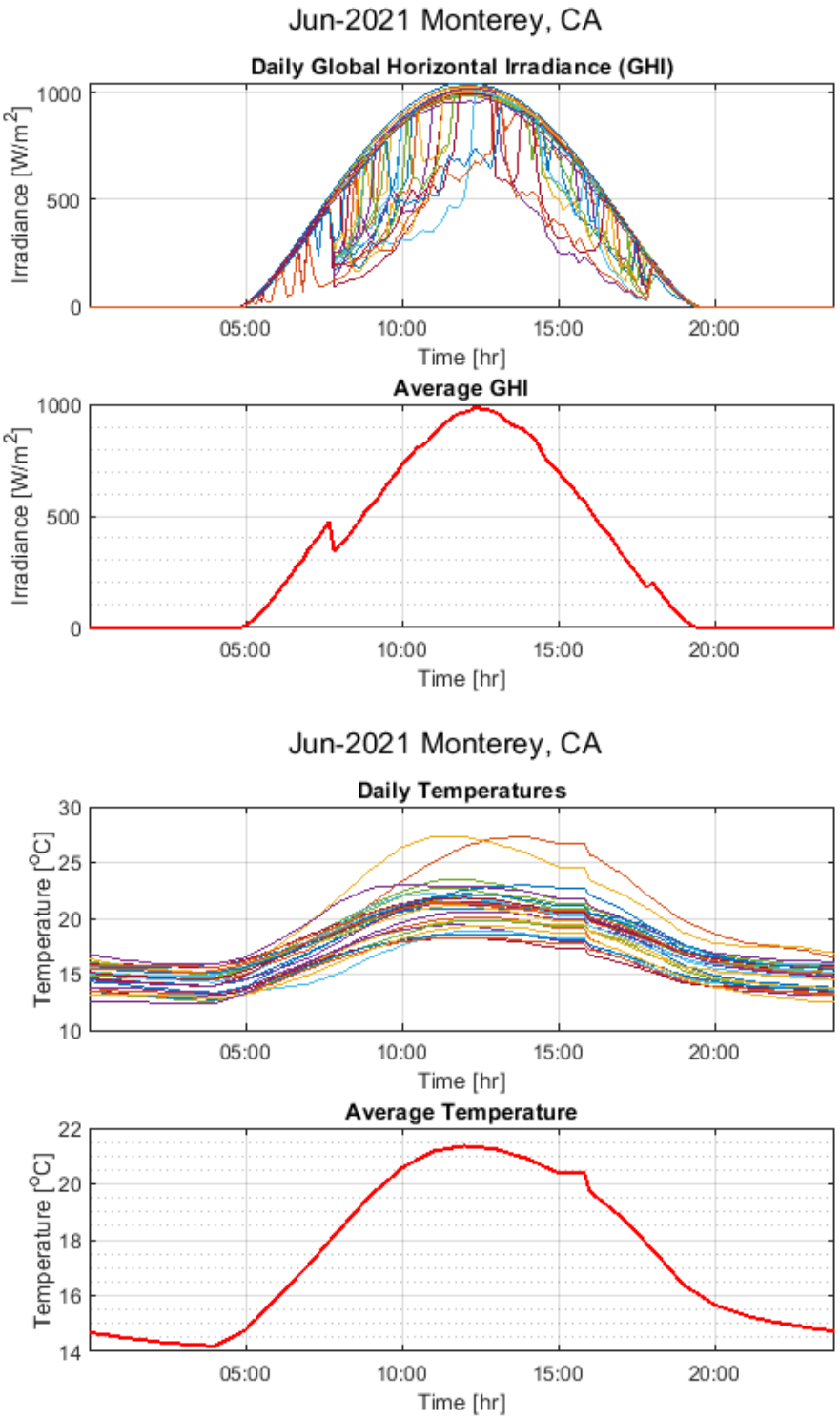

Figure 3.5. Averaged NREL Data

The power output from a PV array can be calculated in terms of GHI and temperature with the specifications of the particular PV panel used. The efficiency of a PV array is computed as the ratio of the maximum power output to the standard test condition irradiance (1000 W/m^2), as shown in (3.6). Incorporating efficiency and temperature compensation (3.7) results in (3.8) as reported by Marion and Smith [16].

$$\eta_{PV} = \frac{P_{max}}{area} / G_{STC} \times 100\% \tag{3.6}$$

$$P_{PV} = \eta_{PV} \times G \times area \times [1 + \alpha(T - T_{STC})] \tag{3.7}$$

$$P_{PV} = P_{max} \times \frac{G}{G_{STC}} \times [1 + \alpha(T - T_{STC})] \tag{3.8}$$

In (3.8) P_{max}, the maximum power, and α, the temperature coefficient, are values specific to each PV panel from its data sheet, and T_{STC} (25 ^oC) is the temperature at standard test conditions. The values for G and T are the averaged values for each irradiance and temperature measurement, respectively, during the day. The predicted PV output, computed for the PV source used in the NPS microgrid (Figure 4.2) is depicted in Figure 3.6. This is the data used in the PV look-up table for the simulations presented in this thesis.

The simulation block "PV Controller" in Figure 3.7 models a solar charge controller. It simply passes the power from the look-up table to the power converter unless the SOC is above 95% in which case it does not continue to charge the battery. This programming models the ideal behavior of a charge controller preventing the battery from overcharging by limiting the PV power contribution when SOC reaches 95%.

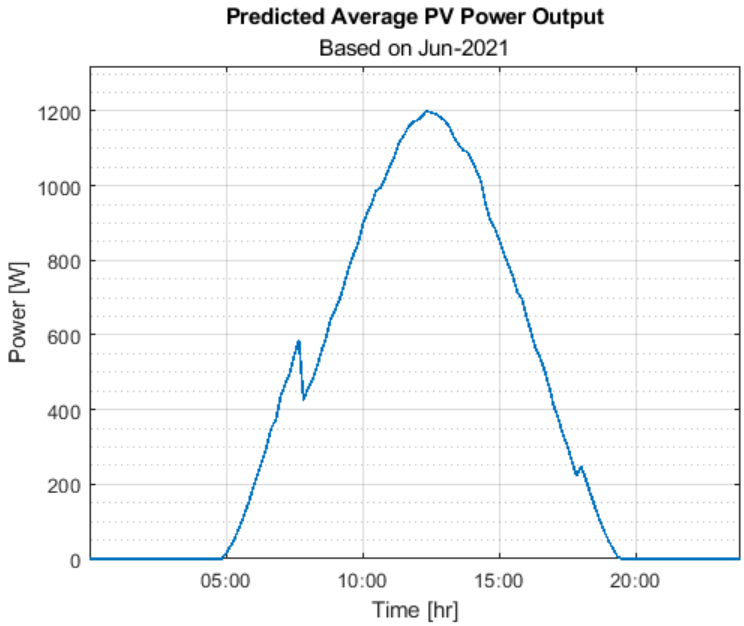

Figure 3.6. Predicted PV Output Power

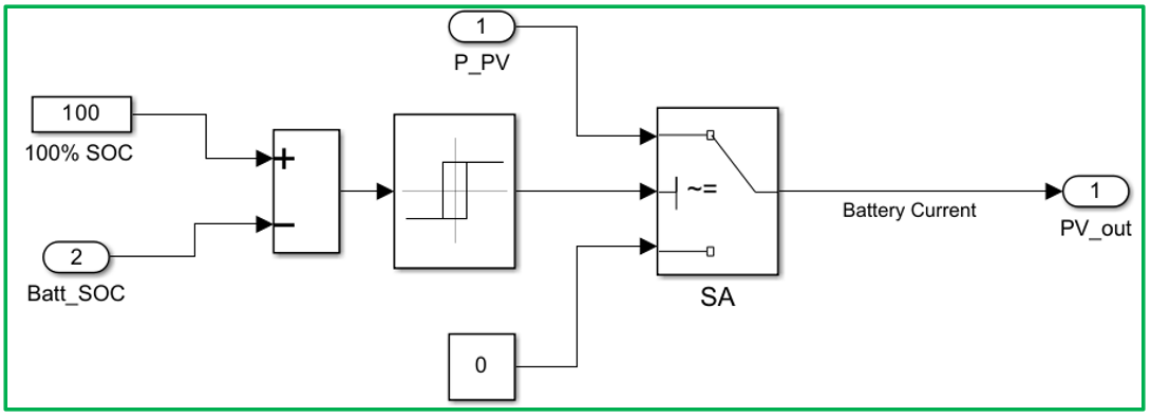

Figure 3.7. Simulink Charge Controller Block

3.2.5 Power Converter

The power converter shown in Figure 3.8 is modeled using (3.5) to calculate the current flowing in or out of the battery bank. Because the current from the solar charge controller does not flow through the inverter/rectifier it is not affected by the inverter efficiency. A

negative battery current indicates power discharging the battery to power the load while a positive battery current indicates that the current is charging the battery.

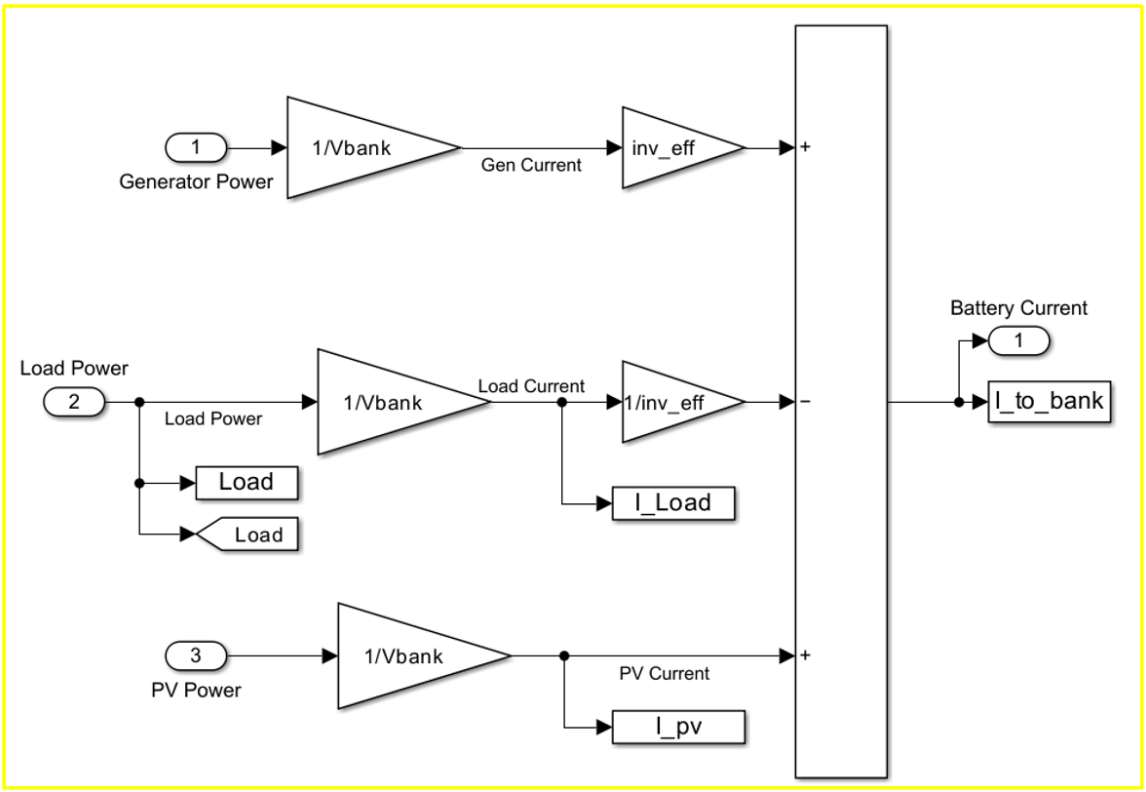

Figure 3.8. Simulink Power Converter Block

3.2.6 Battery Bank

The battery bank serves as an energy storage device and is simulated by integrating the battery current over time divided by overall capacity and battery efficiency of the BESS. Figure 3.9 is a screen capture of Simulink that models SOC of the bank over time.

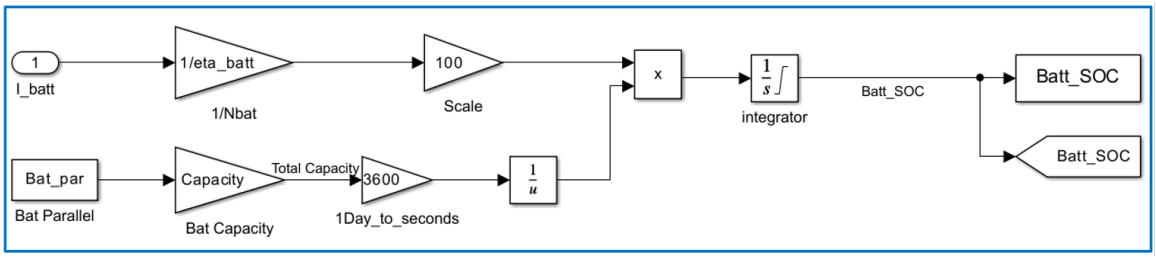

Figure 3.9. Simulink Battery Bank Block

3.3 Simulation Trials

The physics-based model described in the previous sections was used to perform ten trials of simulations which illustrate the microgrid functionality in different scenarios. The simulation parameters are listed in Table 3.1 and are the same for all trials. The "Gen On Signal" and "Gen Off Signal" parameters are the SOC values at which the EMS will signal the back-up generator to start or stop.

Table 3.1. Simulation Parameters

Parameter	Value
Start Time	00:00:00 (Midnight)
Duration	120 hrs (5 days)
PV Panel Efficiency	16.81%
Battery Bank Voltage	24 V
Initial SOC	100%
Gen On Signal	SOC 60%
Gen Off Signal	SOC 95%
Generator Current Limit (AC)	15 A (50% Rated Power)
Inverter Efficiency	90.5%

In Table 3.2, Trials 1, 2, 5, and 8 are performed with the equipment used in the NPS microgrid, including 12 PV panels and a BESS with a 500-Ah capacity. The other trials utilize different sizes of the PV array and BESS to observe the difference in performance. As

described in Section 3.2.4, the output power of the PV array is derived for that geographic location based on NREL data. The load profile used in Trials 2 through 8 is a scaled load power profile mimicking one measured by the United States Marine Corps (USMC) on a typical FOB [17]. The original and scaled profiles are depicted in Figure 3.10. The load power is scaled to fit the NPS microgrid design and DER ratings.

Table 3.2. Simulation Trials

Trial	Location	PV Array Size	BESS Capacity	Power Load
Trial 1	Monterey, CA	12 Panels	500 Ah	1000 W (Constant)
Trial 2	Monterey, CA	12 Panels	500 Ah	FOB Load Profile
Trial 3	Monterey, CA	12 Panels	2000 Ah	FOB Load Profile
Trial 4	Monterey, CA	24 Panels	2000 Ah	FOB Load Profile
Trial 5	Key West, FL	12 Panels	500 Ah	FOB Load Profile
Trial 6	Key West, FL	12 Panels	2000 Ah	FOB Load Profile
Trial 7	Key West, FL	24 Panels	2000 Ah	FOB Load Profile
Trial 8	Seattle, WA	12 Panels	500 Ah	FOB Load Profile
Trial 9	Seattle, WA	12 Panels	2000 Ah	FOB Load Profile
Trial 10	Seattle, WA	24 Panels	2000 Ah	FOB Load Profile

The assumptions described next are made to simplify the simulation. First, the voltage of the battery bank is treated as a constant value while the voltage of a real battery will fluctuate according to its charge. Second, the simulation assumes the solar charger and the inverter can both supply current simultaneously to the battery bank to charge it.

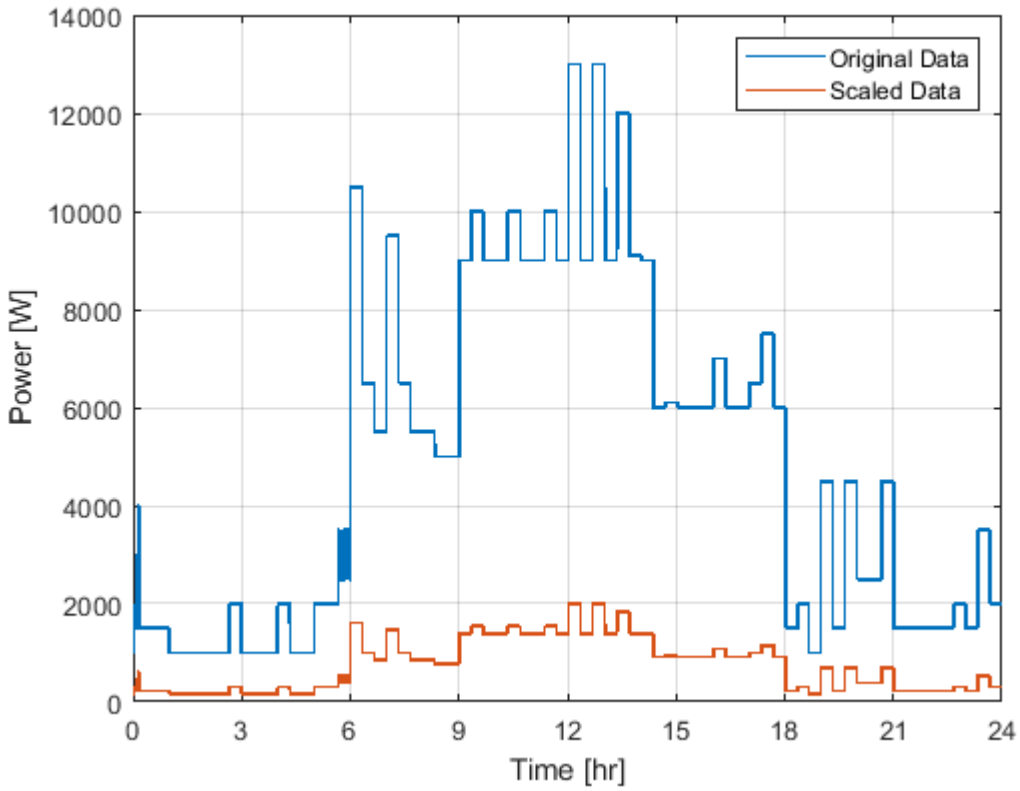

Figure 3.10. Measured and Scaled Load Profiles

3.3.1 Simulated Trials in Monterey, California

The first four trials are simulated in Monterey, CA. Trial 1 is obtained with 12 solar panels and 12 2-V batteries rated at 500 Ah to replicate the equipment used at the NPS microgrid. A constant 1-kW load is used to set a baseline performance for the microgrid. The simulation results for Trial 1 are depicted in Figure 3.11. It presents the power contributed by each component of the microgrid. The negative power values on the graph represent power flowing out of the system and positive values represent flowing into the into the system. As such the load power is negative in the graph. As designed, the power flowing in and out of the BESS is a combination of the other components shifted by the efficiency of each. The bottom plot of the figure shows the SOC of the BESS and marks where the EMS signals the generator to start and stop.

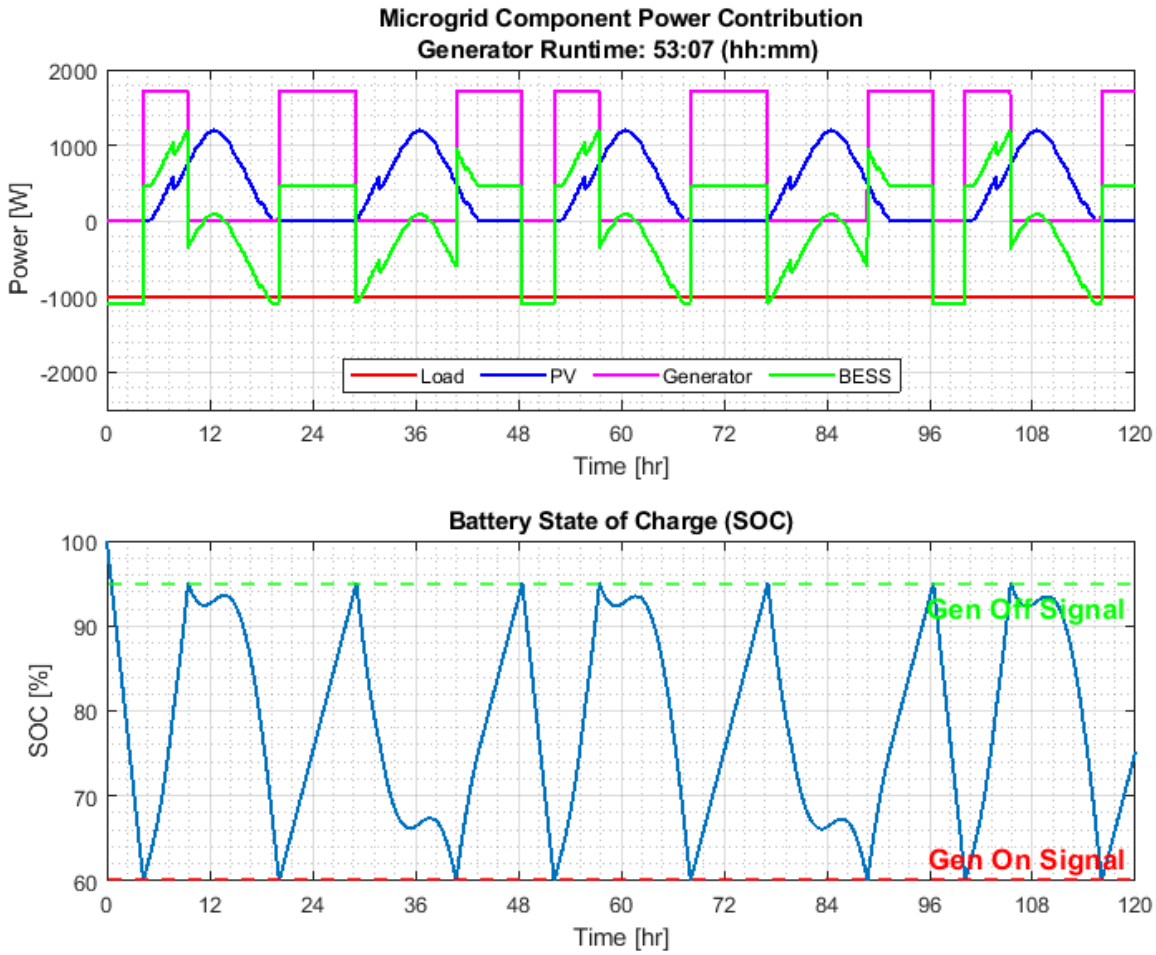

Figure 3.11. Trial 1 Results

The results from Trial 2 are shown in Figure 3.12, where the response of the microgrid with a more realistic load profile is displayed. This load peaks at 2 kW with an average value of approximately 750 W. The generator is active almost 32 h over the 120-h duration. After 24 hours, the system seems to enter a repeating cycle where the generator starts about the same time every day. Trial 3 produces the simulations in Figure 3.13 and shows the effect that increasing the capacity of the BESS by a factor of four has on the microgrid functionality. In practice, this can be accomplished by installing three more sets of battery cells in parallel. It is observed that the BESS takes much longer to discharge, now lasting almost 40 hours without engaging the generator. Conversely, recharging also takes longer, but the generator is started on fewer occasions. Trial 3 results in the generator running about 11% less than

Trial 2, which would also imply a proportional 11% in fuel cost savings in a five-day period.

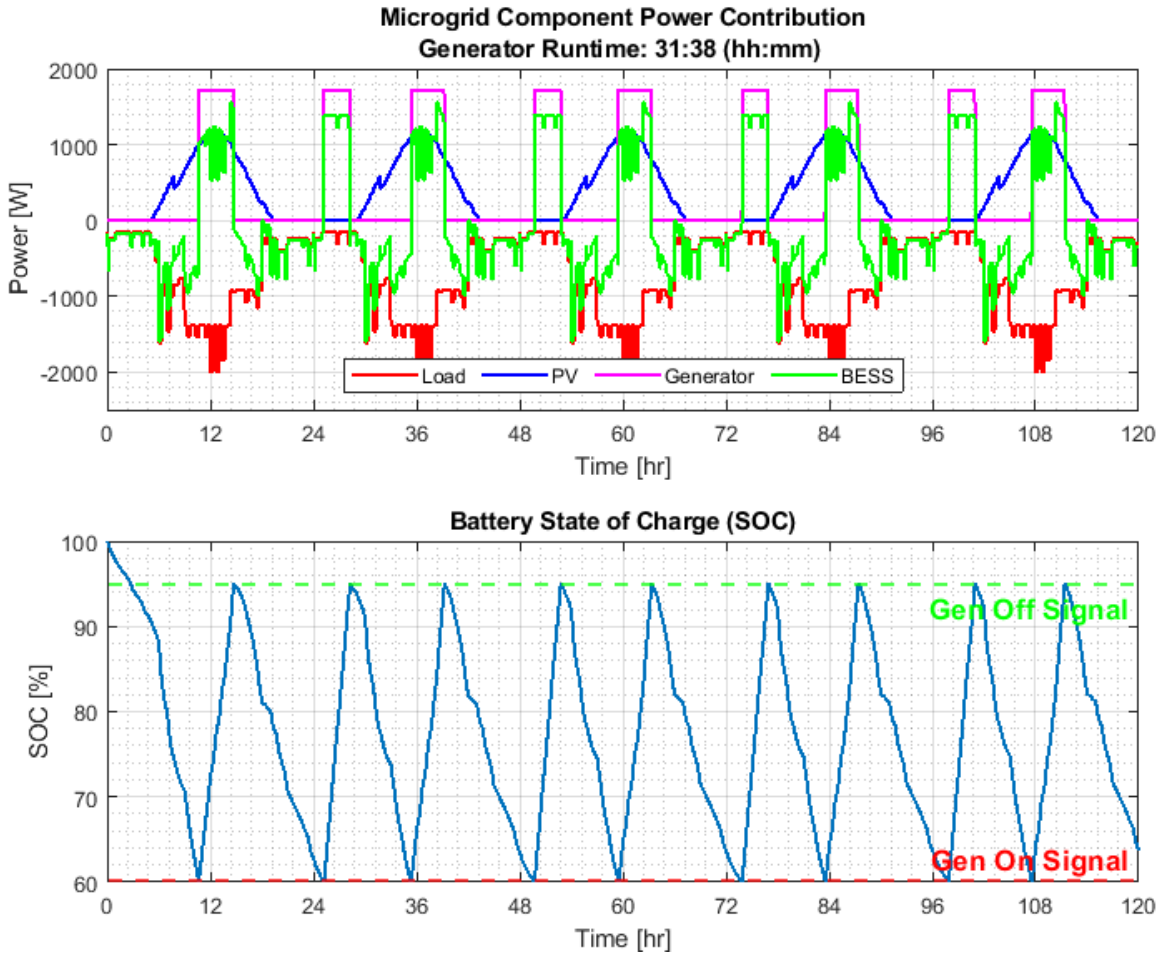

Figure 3.12. Trial 2 Results

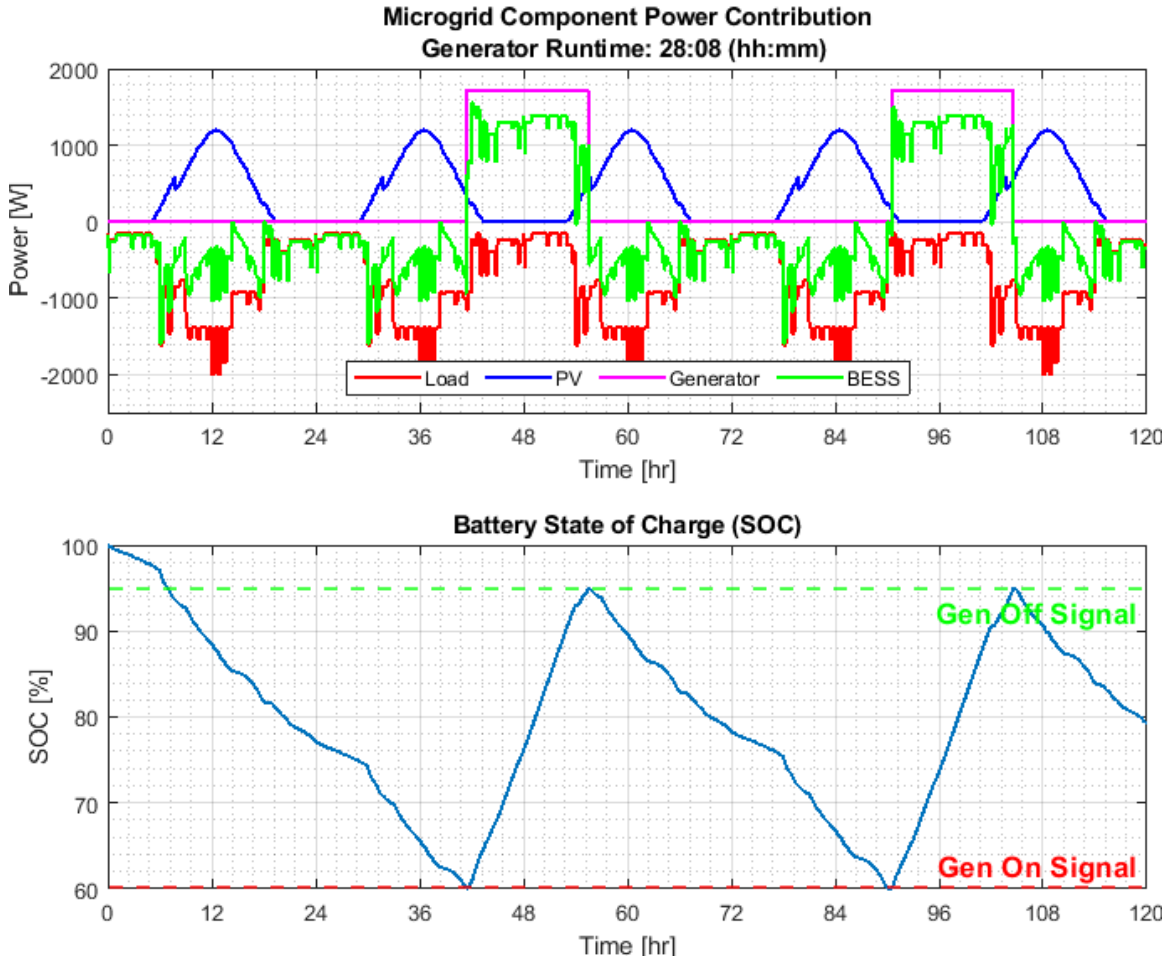

Figure 3.13. Trial 3 Results

Next, with a larger BESS, Trial 4 demonstrates how increasing the size of the PV array further decreases reliance on the generator. In this simulation, the generator never receives a signal to start. Running the simulation for a longer time period would show that the SOC would not reach the minimum point until after 11 days. It is valuable to note one of the benefits of a larger BESS comes when the power load peaks it does not quickly deplete the SOC causing the generator to start. This characteristic allows the renewable energy sources to carry the majority of the load versus the non-renewable sources. In this trial, the doubled size of the PV array resulted in a PV power contribution high enough for the solar charger to curtail its power because the BESS SOC reaches 100% near hour 14.

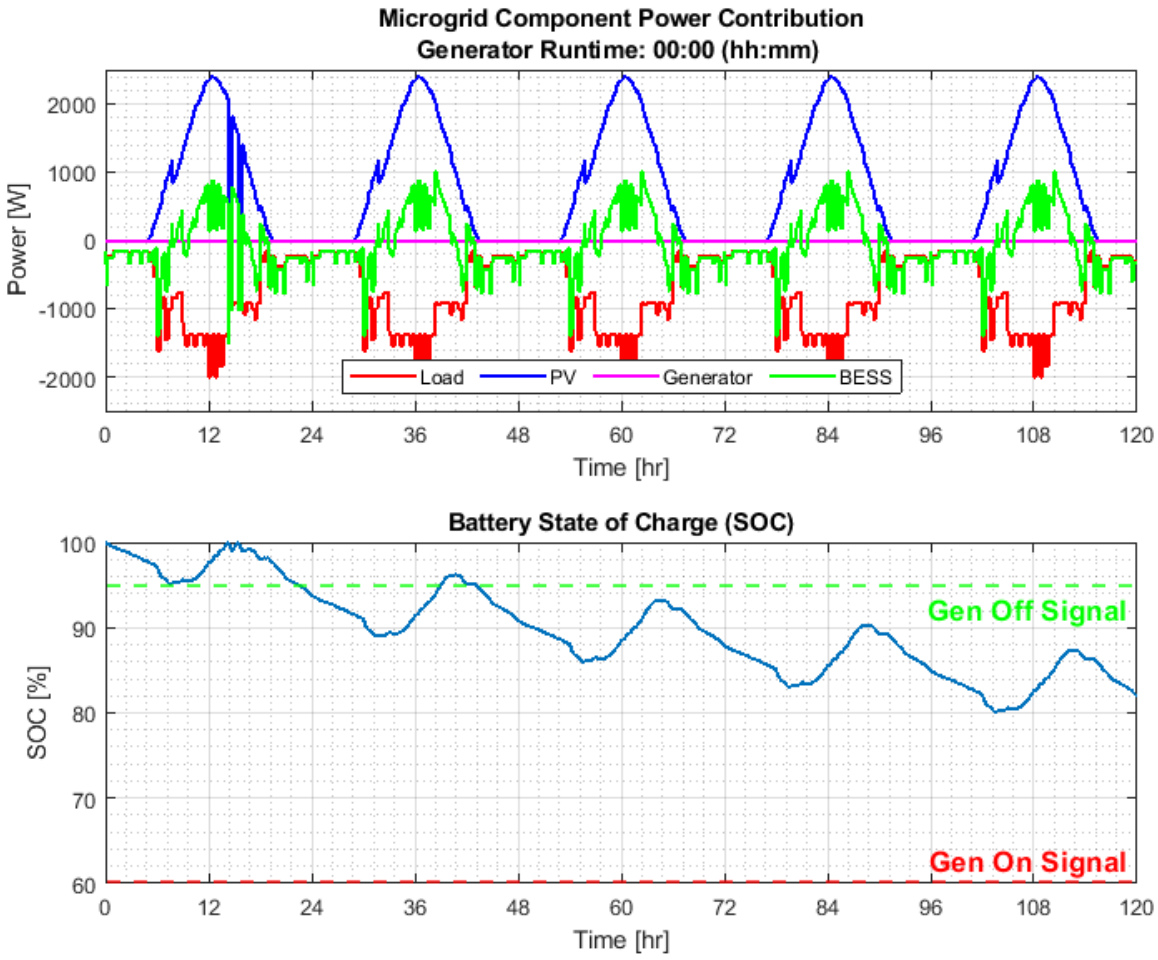

Figure 3.14. Trial 4 Results

3.3.2 Simulated Trials in Key West, FL

For the trials simulated in Key West, FL, once again the NREL irradiance data was processed to determine an expected PV power output. The outputs depict a similar trend as the those in Monterey, CA, with the main difference being the different contribution of solar energy.

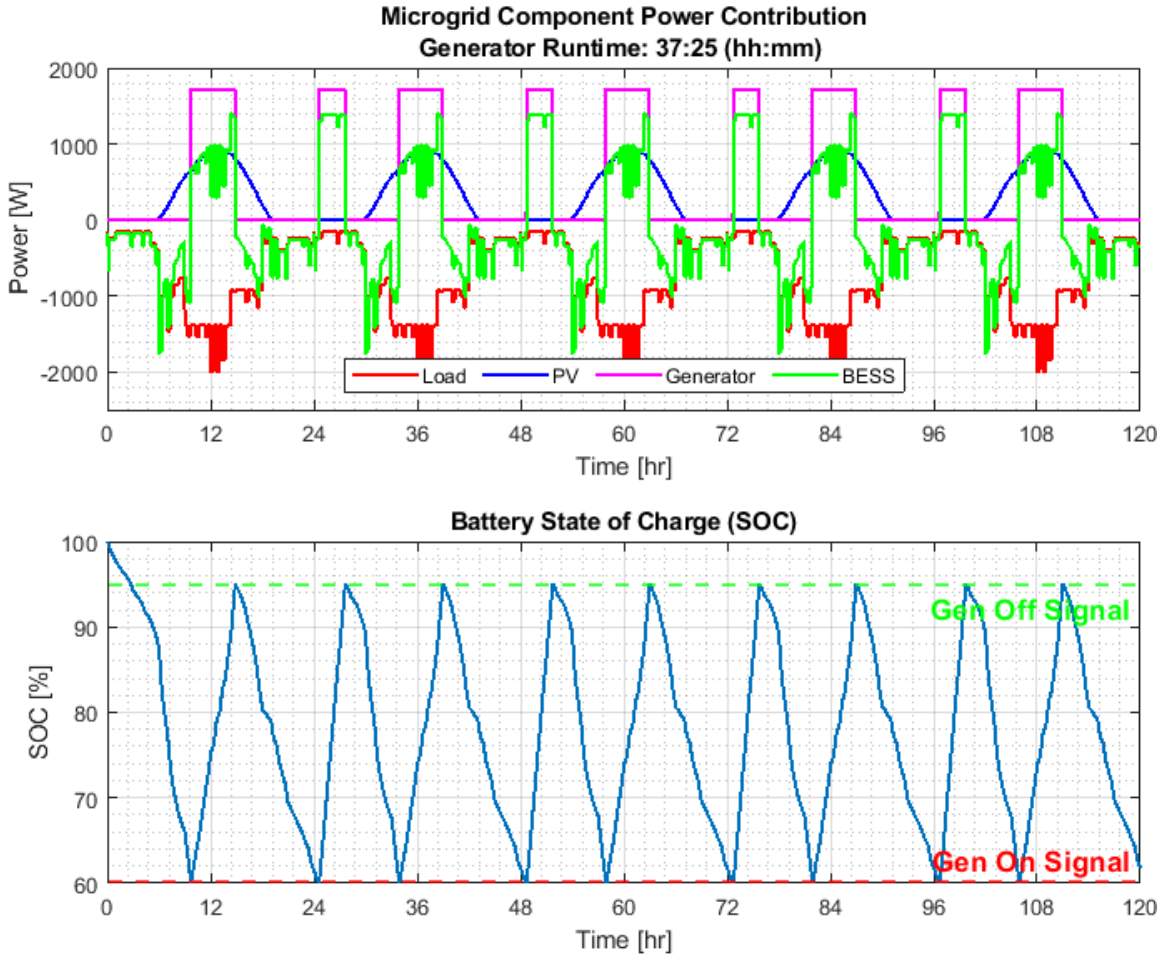

Figure 3.15. Trial 5 Results

The simulations obtained for Key West, FL, suggest that although the geographic location is more tropical, they do not necessarily imply that the solar power contribution will be higher. With 12 panels for Monterey, CA the PV contribution peaked around 1200 W; whereas in Key West, FL it peaked around 950 W. This could be due to higher ambient and panel temperatures causing greater loss suggested by the negative value of the temperature coefficient in (3.8). Trial 6 results, shown in Figure 3.16, shows a shorter generator run time, about 17% shorter than Trial 5.

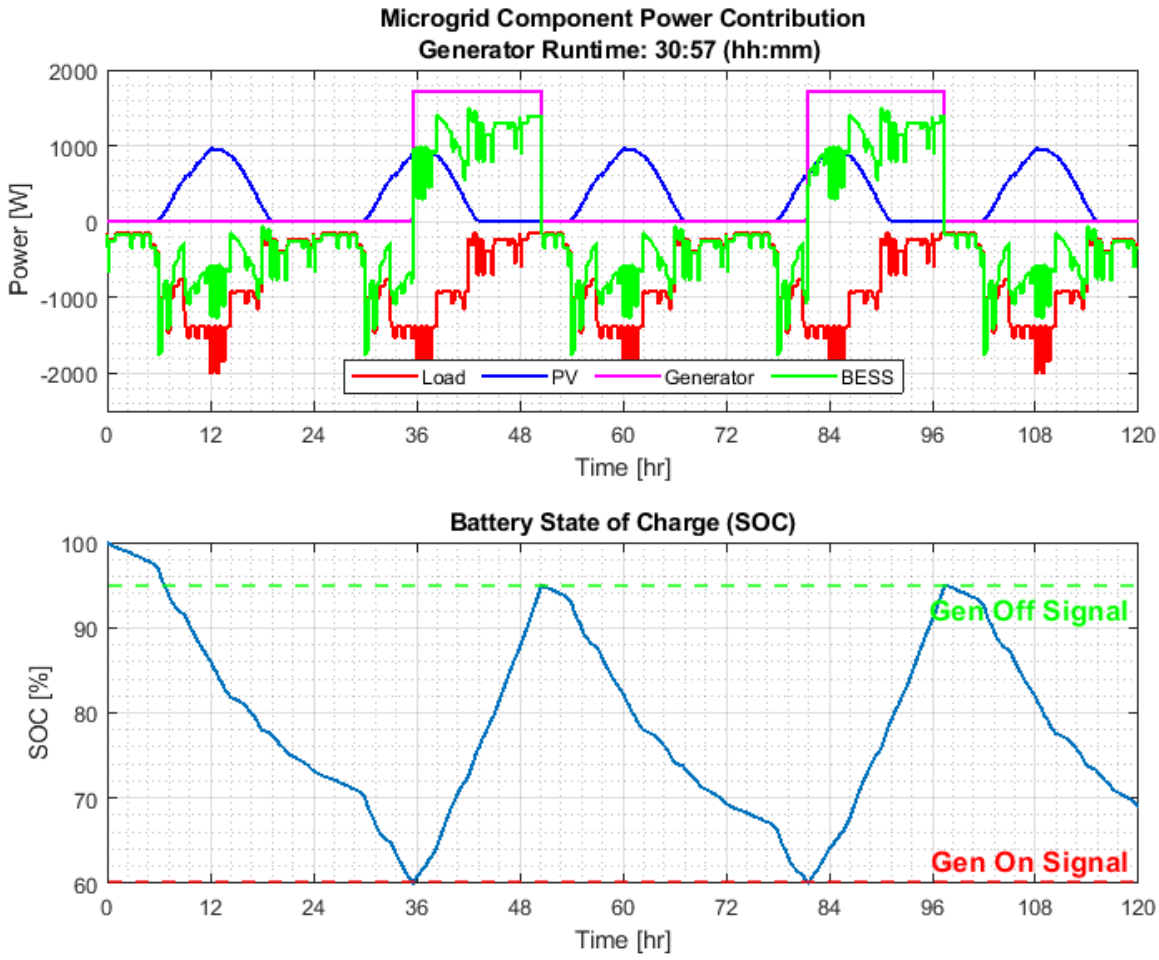

Figure 3.16. Trial 6 Results

Figure 3.17 shows the results of Trial 7 performing better than Trial 6. The generator run time is about 70.7% less than Trial 5 over the five-day period. Again, this would translate to about 70% in fuel cost savings.

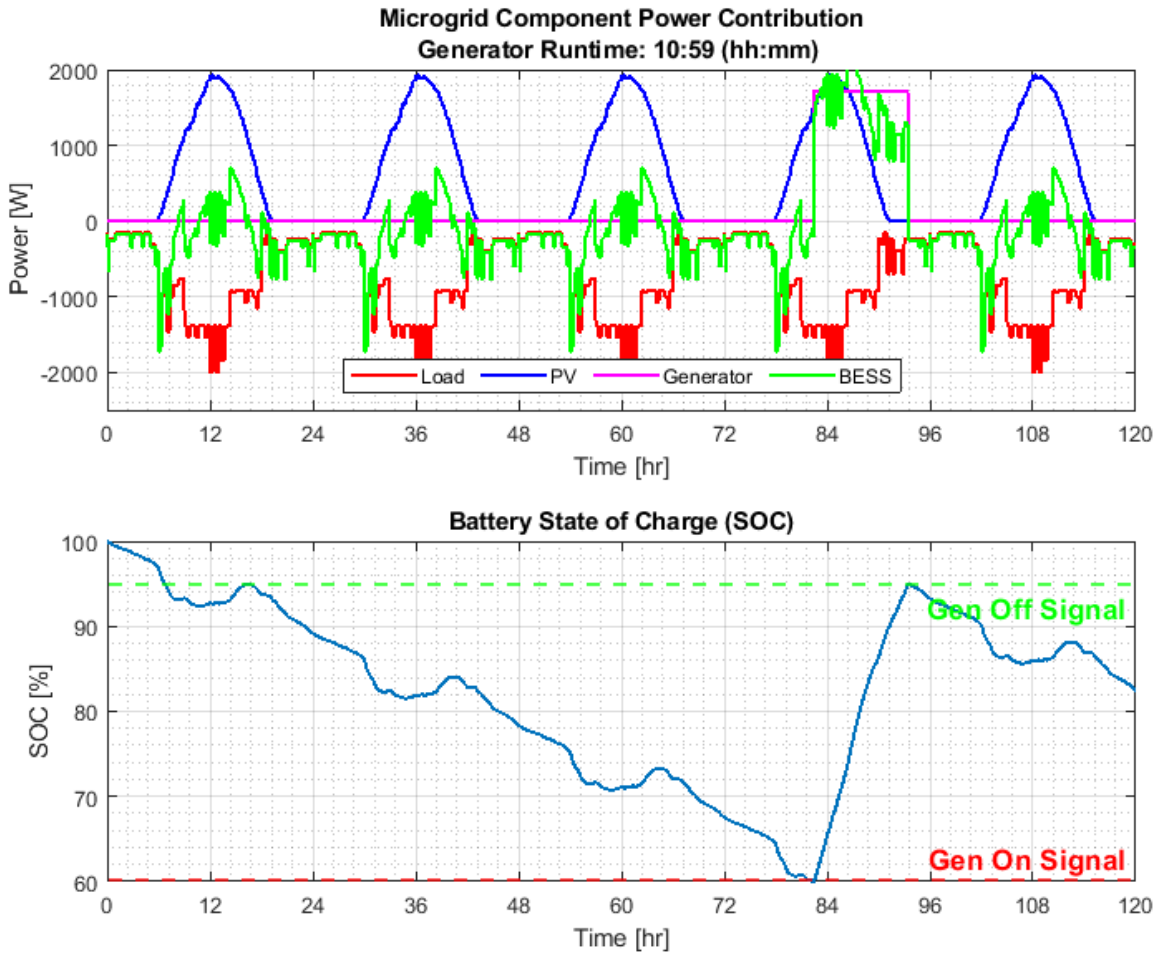

Figure 3.17. Trial 7 Results

3.3.3 Simulated Trials in Seattle, WA

Running the simulation now with solar data for a northern climate in Seattle, WA, yielded the results in the following figures. The solar power peaked around 1000 W, between the data for Monterey and Key West. Overall, the trend is the same from the previous trials. The results for Trial 8 are shown in Figure 3.18 and serve as the baseline for the following two trials. The generator ran almost 36 h during the 120-h simulation.

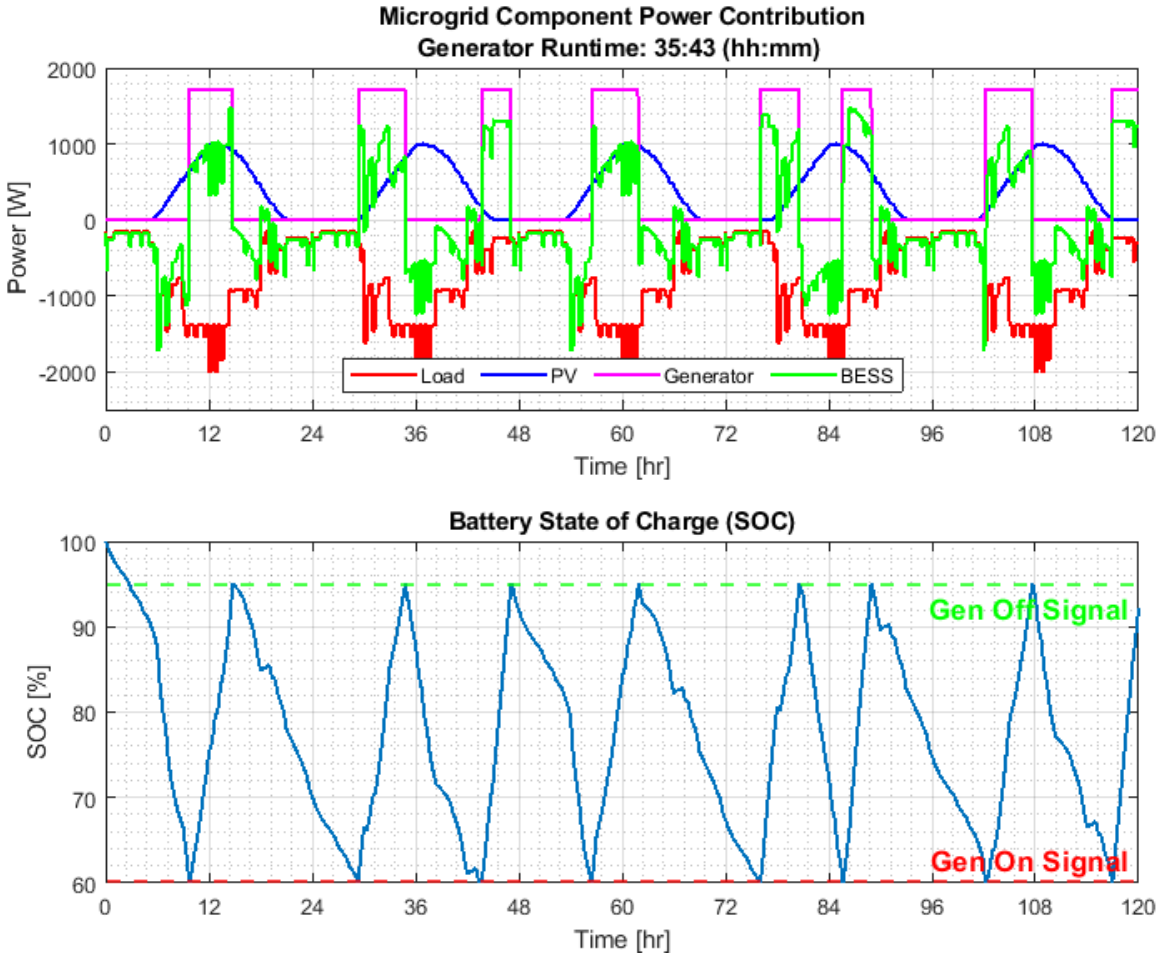

Figure 3.18. Trial 8 Results

Figure 3.19 shows the results of increasing the size of the BESS. It reports a 22.4% shorter generator run time over the five days. The generator does not get started by the EMS until after 36 h into the simulation.

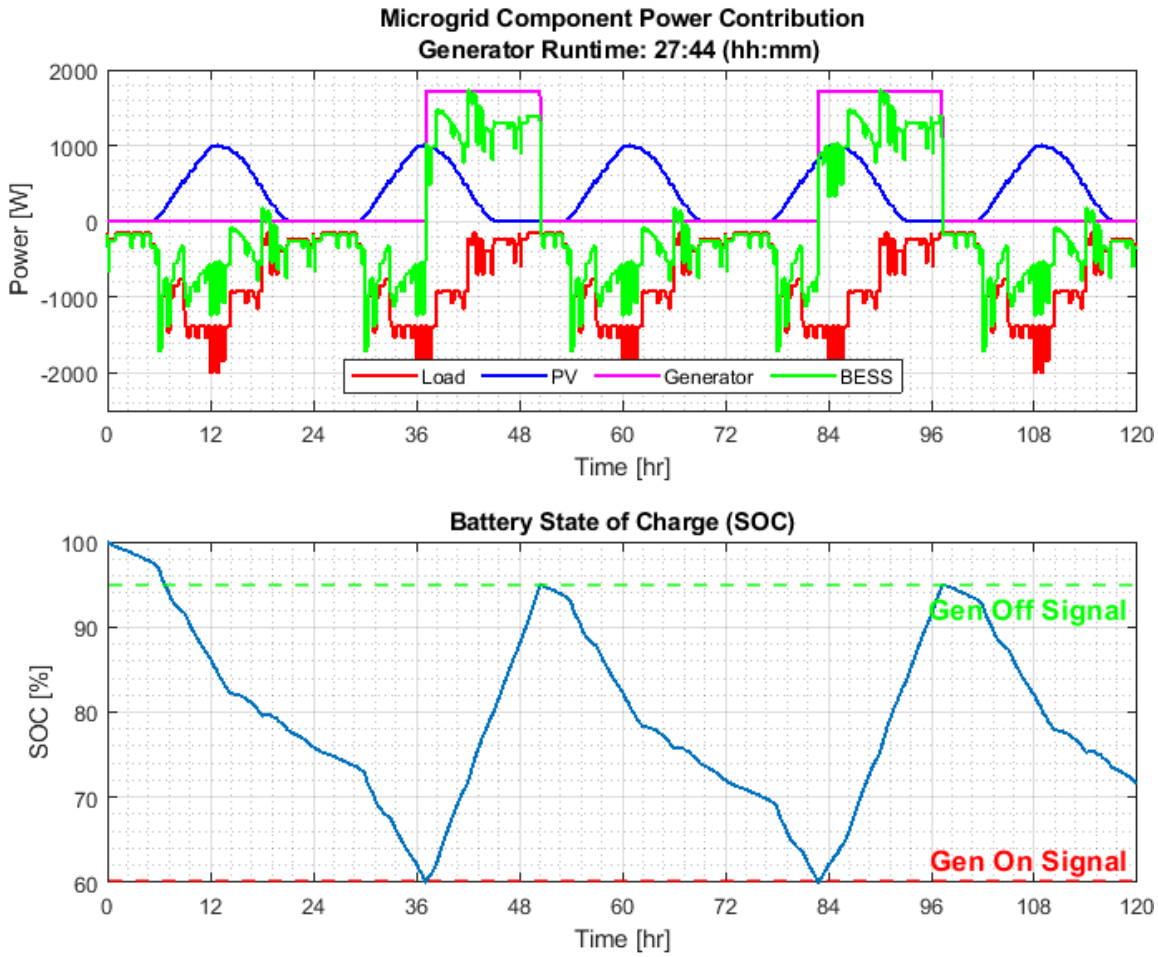

Figure 3.19. Trial 9 Results

In the results for Trial 10, shown in Figure 3.20, the generator is not started in the first 120 s when the PV array size is doubled. The results again highlight the benefit of increasing the energy storage systems to buffer the peaks in the load profile.

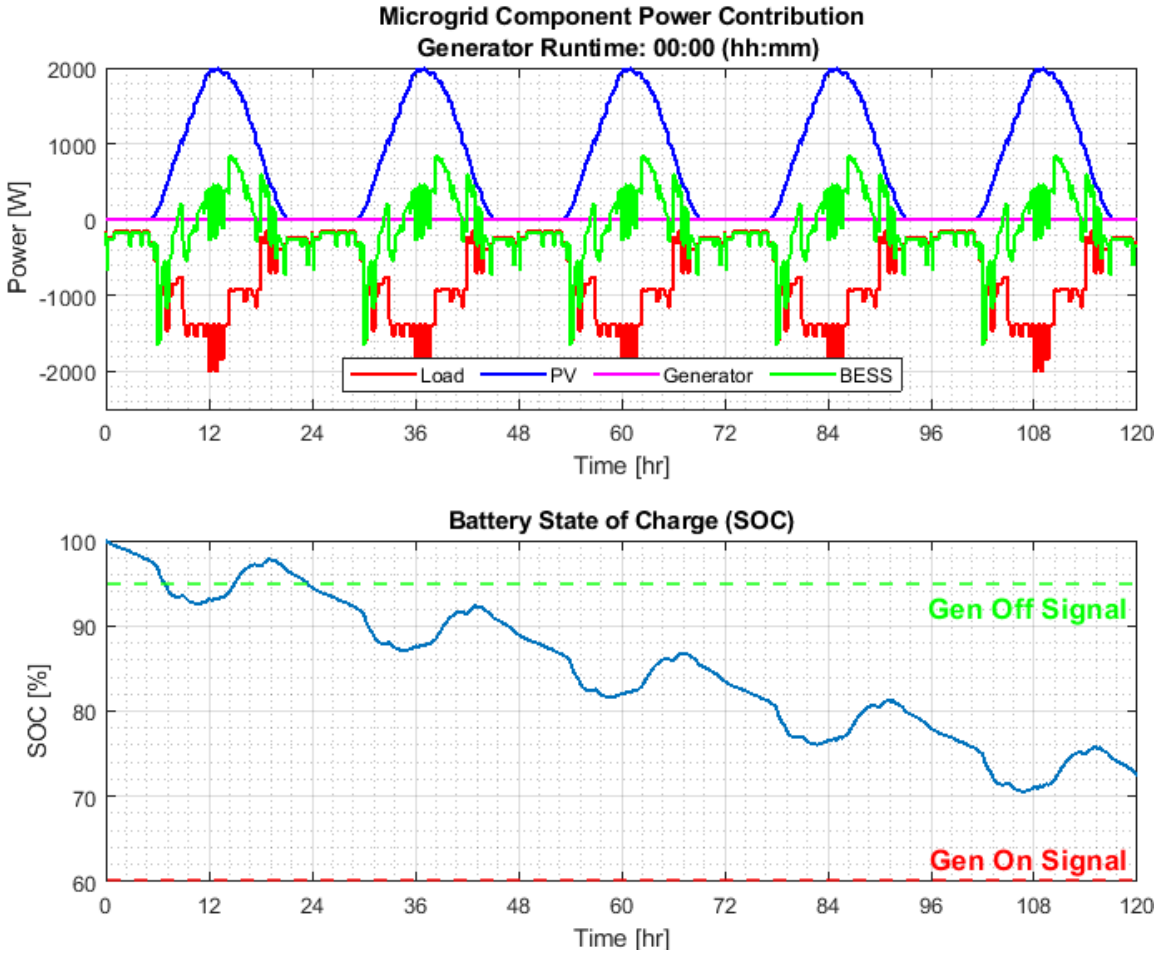

Figure 3.20. Trial 10 Results

CHAPTER 4:
Experimental Results and Model Validation

Having completed the various trials of the physics-based model in Chapter 3, this chapter explores how the simulated results compare to the experimental trials. This chapter presents the architecture and components of the NPS microgrid before comparing the results of the experimental measurements to the simulated results.

4.1 NPS COTS Microgrid Architecture

Figure 4.1 is a schematic diagram of the COTS microgrid used at NPS for microgrid experimental research. The black lines represent the power flowing from one component to another. The blue lines represent communication lines to control the different components. The first components to note are the different energy sources. These sources are a PV array, a generator, and the utility grid. As the NPS microgrid is currently configured, the power converter cannot receive power from the utility grid and the generator simultaneously. The EMS is the controling mechanism of the microgrid which schedules the microgrid resources to ensure power to the load at all times. It prioritizes energy sources or manages a desired operating profile. It monitors availability of energy in the battery bank and the power output of the PV array, and it can engage generator or grid power for support. The charge controller maximizes the available power output from the PV arrays and regulates it to charge the battery bank. The generator start module is often integrated with the generator but can be a separate unit. It receives signals from the EMS to start or stop the generator. The battery bank plays an important role in conjunction with the renewable energy sources. Because renewable energy sources do not reliably provide constant power, an energy storage device such as a battery bank will bridge the gap when no power from solar or wind is being delivered. The energy storage system can also recharge with excess power when the generator is turned on to support the system.

Delivering power to the load is the power converter, which is a crucial component to the operation of the microgrid. Because the different energy sources are both DC and AC systems, the power converter will either invert or rectify the power depending on the

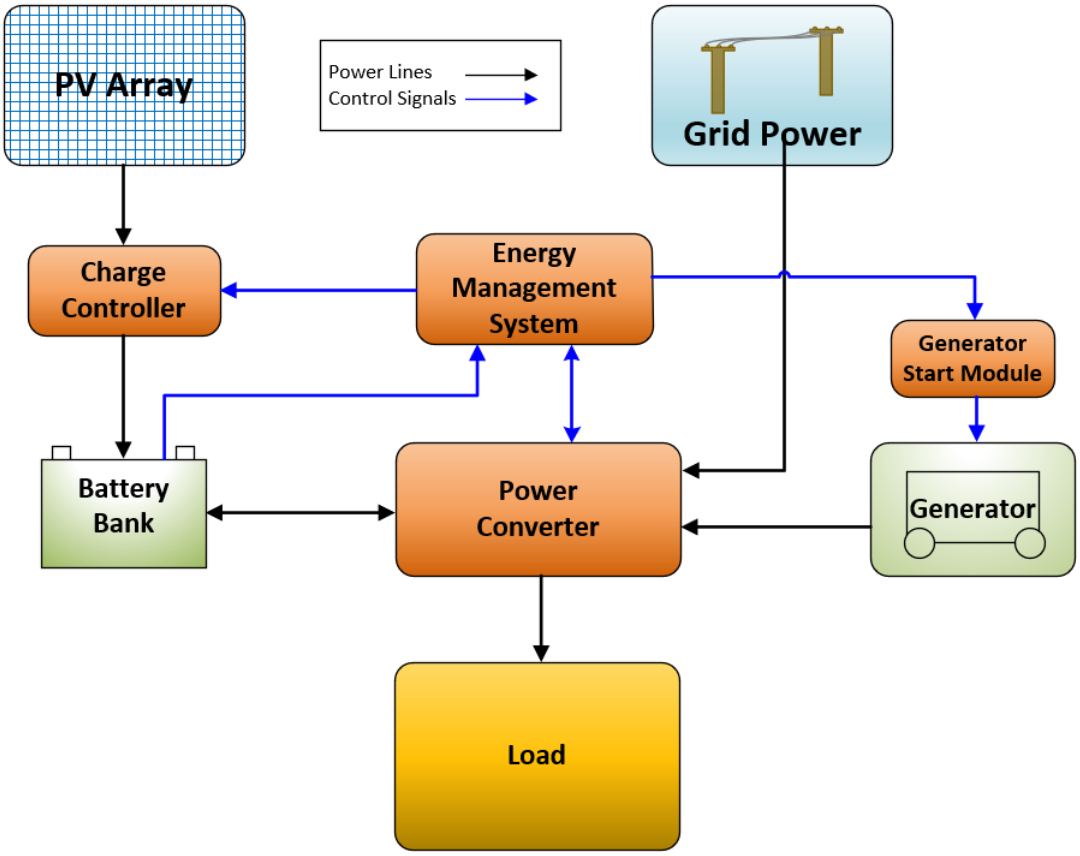

Figure 4.1. Microgrid Architecture

direction of the current. During normal operation, the power converter will take DC power from the battery bank and invert it into AC power for the load. The power converter may need to stop taking power from the battery bank for two main reasons: the bank does not have enough charge or the load begins drawing more power than the bank can provide. In these events, the EMS will signal the generator to start or signal the power converter to begin receiving power from the grid. The power converter will use the AC power to feed the load and rectify any excess power to charge the battery bank.

4.2 NPS COTS Microgrid Components

This section presents the equipment specifications of the NPS microgrid which is used to validate the modeling and simulations discussed in Chapter 3.

4.2.1 PV Array

The solar panels used to build the PV array are manufactured by High Quality Solar Technology (HQST). Each panel has a maximum power output of 100 W. The array is configured into three strings of four panels each with a total maximum power output of 1200 W. The panels face south directed at approximately 170° and have an inclination of 30°.

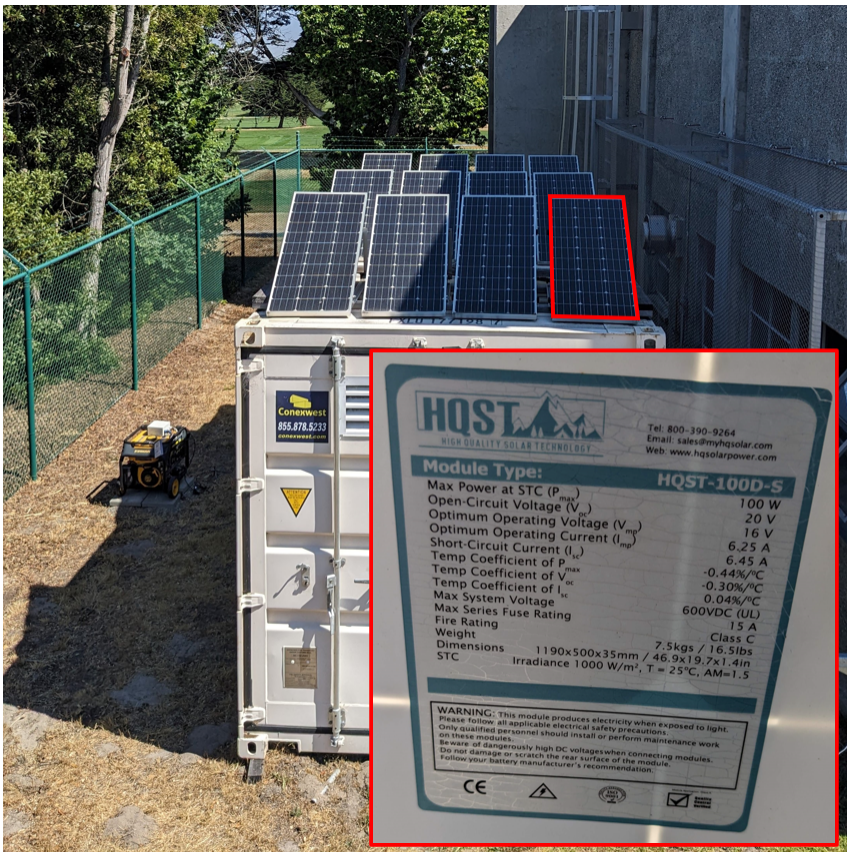

Figure 4.2. NPS COTS PV Array

4.2.2 Charge Controller

Outback Power manufactures the FLEXmax 80 solar charger controller used in this microgrid [18]. It employs maximum point power tracking (MPPT) technology to maximize the power output of a given PV array.

4.2.3 Battery Bank

The battery bank uses twelve 2-V cells to create a 24-V energy storage system. SLR500-2 is a 2-V, 500-Ah lead-carbon battery made by GS Yuasa [19]. The cells are configured in series to create a 24-V system with a 500-Ah capacity.

Figure 4.3. NPS Microgrid Setup

4.2.4 Generator

The generator used in this microgrid is a Firman H03651, a dual-fuel gasoline or propane generator with a running output of 3650 W [20]. For this thesis the generator is fueled with gasoline. To allow this generator without auto-start capability to be controlled by the EMS it has been coupled with a controller, GSCM-Mini 60 Hz, made by Atkinson Electronics, Inc [21]. Some modification had to be made to the manual carburetor choke to allow the generator to start autonomously. This modification included an Arduino board to monitor the signal sent by the generator start control module and a servo to actuate the carburetor choke. More detailed information on this modification is in the appendix.

Figure 4.4. Generator and Controller

4.2.5 Power Converter

Also manufactured by Outback Power is the VFXR3524A Inverter/Charger which serves as the power converter in this microgrid [22]. This vented model has a continuous power rating of up to 3500 VA. It is mounted together with the solar charge controller and the MATE3s (EMS) as seen in the left photograph of Figure 4.3.

4.2.6 Energy Management System

The EMS for this microgrid is the MATE3s [23]. It monitors incoming power from the PV array and AC inputs (generator or utility grid power), battery bank voltage, and power output to the load. By monitoring these inputs and outputs, it coordinates the various resources to provide uninterrupted power to the load. MATE3s also allows the user to program different profiles into it to dictate how the microgrid will operate. It can be operated in three different modes: Grid Tied, Off-Grid, and Backup. In Grid Tied mode, the system will sell excess power to the grid or, if the battery bank charge is too low, will buy power from the grid. Off-grid mode operates in the islanded configuration with no tie to the utility grid. In Backup mode, the microgrid only provides power to the load if grid voltage waveform become abnormal [7] or is interrupted.

The MATE3s is set to default programming to comply with IEEE Standard 1547. This ensures power sold to the utility grid does not fall outside the specifications for voltage or frequency abnormalities. Conversely, it also monitors input AC power sources to the system so that if any disturbances in voltage or frequency occur, the EMS will disconnect and not attempt to reconnect until the standard conditions are met.

For this thesis the microgrid is operated in the Off-Grid mode and uses the advanced generator start (AGS) feature to incorporate the generator. AGS can start and stop the generator with a 12-V signal based off several different criteria including battery voltage, battery SOC, load demand, and timing schedule. The trials run in this exercise used battery SOC as the sole criteria to engage the generator.

4.2.7 Load

In order to standardize the experimental trials, a programmable load was used and the power drawn by the load was set to a constant value. The Kepco load and programmable power supply shown in Figure 4.5 allows the user to set the load at a specific power usage to better observe the performance of the system.

4.2.8 Data Acquisition

The MATE3s has data logging capability for the majority of the measurements needed in this study. It measures voltage, current, and power from the PV array; voltage, current, and

SOC of the battery bank; and voltage and current from the input AC sources. The logging time interval can be set by the user and it was set to 10 seconds for this thesis.

The only data that is not directly logged by the MATE3s is the current and therefore power, drawn by the load. To measure and log this data the Fluke 434 Power Analyzer with the same time interval is used. The power analyzer is used to measure voltage, current, power factor, and power that the electronic load is drawing from the microgrid.

Figure 4.5. Electronic Load and Power Analyzer

4.3 Experimental Measurements and Model Validation

The COTS microgrid described in the previous section was operated in islanding mode in two different three-days trails to collect experimental data. The measured results were compared to the simulated results to validate the physics-based model presented in Chapter 3. For clarity of reference, Table 4.1 identifies the input properties for each comparison in both experimental trials. Measured Trial 1 Load is depicted in Figure 4.6, and Measured Trial 2

Load is depicted in Figure 4.11.

Table 4.1. Experimental Trials and Simulation Comparisons Reference

Comparison	Simulation Load Input	Simulation PV Input
Power Comparison 1 (Fig 4.7)	Measured Trial 1 Load	Trial 1 Measured PV
SOC Comparison 1 (Fig 4.8)	Measured Trial 1 Load	Trial 1 Measured PV
Power Comparison 2 (Fig 4.9)	Measured Trial 1 Load	NREL PV Data
SOC Comparison 2 (Fig 4.10)	Measured Trial 1 Load	NREL PV Data
Power Comparison 3 (Fig 4.12)	Measured Trial 2 Load	Trial 2 Measured PV
SOC Comparison 3 (Fig 4.13)	Measured Trial 2 Load	Trial 2 Measured PV
Power Comparison 4 (Fig 4.14)	Measured Trial 2 Load	NREL PV Data
SOC Comparison 4 (Fig 4.15)	Measured Trial 2 Load	NREL PV Data

4.3.1 First Experimental Trial

For the first experimental trial, the NPS microgrid was operated over a period of three days in June in order to observe how the system performed in comparison to the physics-based model. The Kepco DC electronic load was programmed to draw a constant 500 W from the power converter. Figure 4.6 is a plot of the power drawn by the electronic load and measured by the Fluke 343 Power Analyzer.

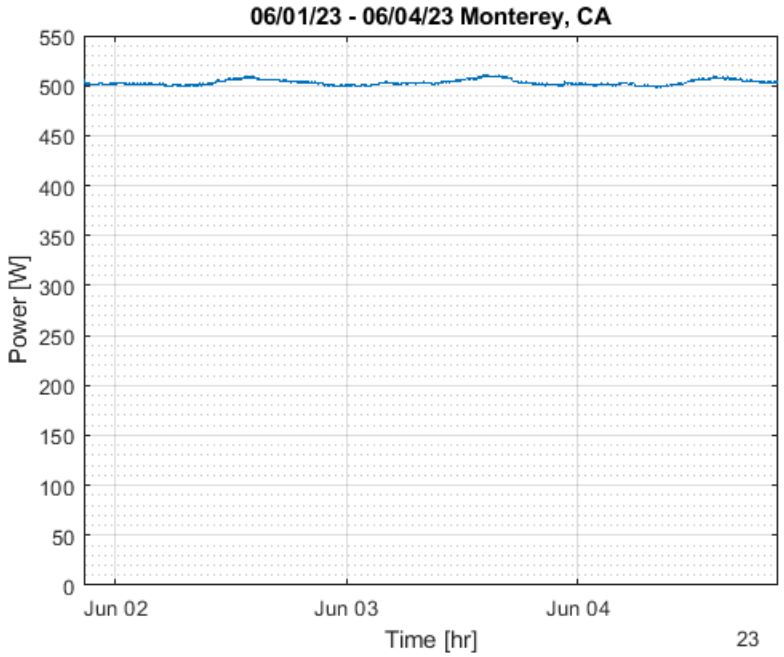

Figure 4.6. Power Drawn by the Load in the First Experimental Trial

At the end of the experiment, the data was downloaded from the MATE3s data logger and used to plot the power waveforms for each component. The same load and generator power profiles used in the hardware were used to run a simulations which was compared to the experimental measurements.

Simulation with Experimental PV Profile Input

For the first comparison, the power measured at the PV array was used as the PV input for the simulation. Figure 4.7 shows the experimental measurements and the results of the simulation in comparison to better visualize the accuracy of the physics-based model.

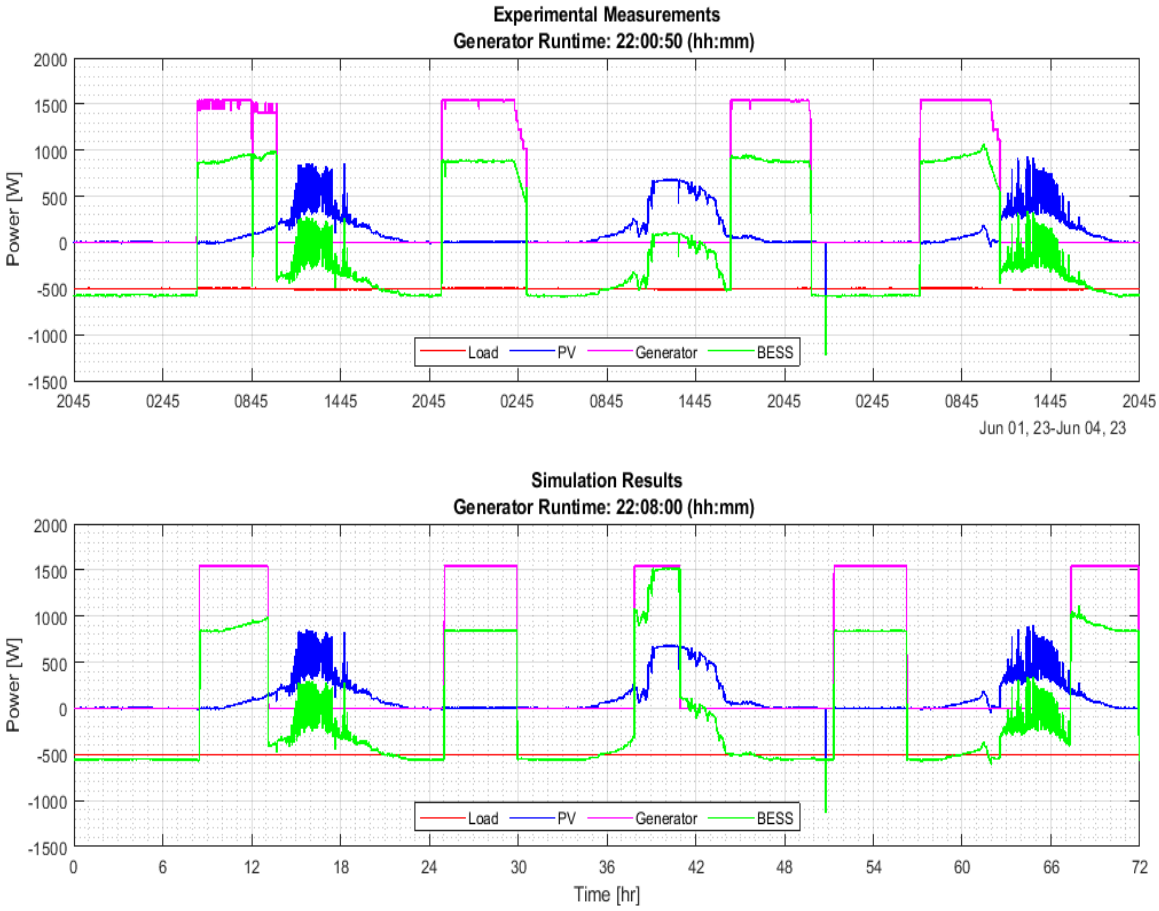

Figure 4.7. Experimental vs. Simulated Power Comparison 1

Both the experimental measurements and the simulations match up until about hour 38 when the simulated EMS activates the generator, while the hardware does not. However, the generator is on in both cases for a similar amount of time with only a seven minute difference approximately. This difference could be explained by the generator signal being determined by SOC. Figure 4.8 compares the measured and simulated SOC showing that the hardware EMS resets the SOC to 100% at the end of the charging cycle. Had the value not been reset, it is plausible that the generator would have been signaled to activate approximately 1145 on June 2. Regardless, the rates of change of the SOC in the simulation matches well the experimental measurements, validating the physics-based model.

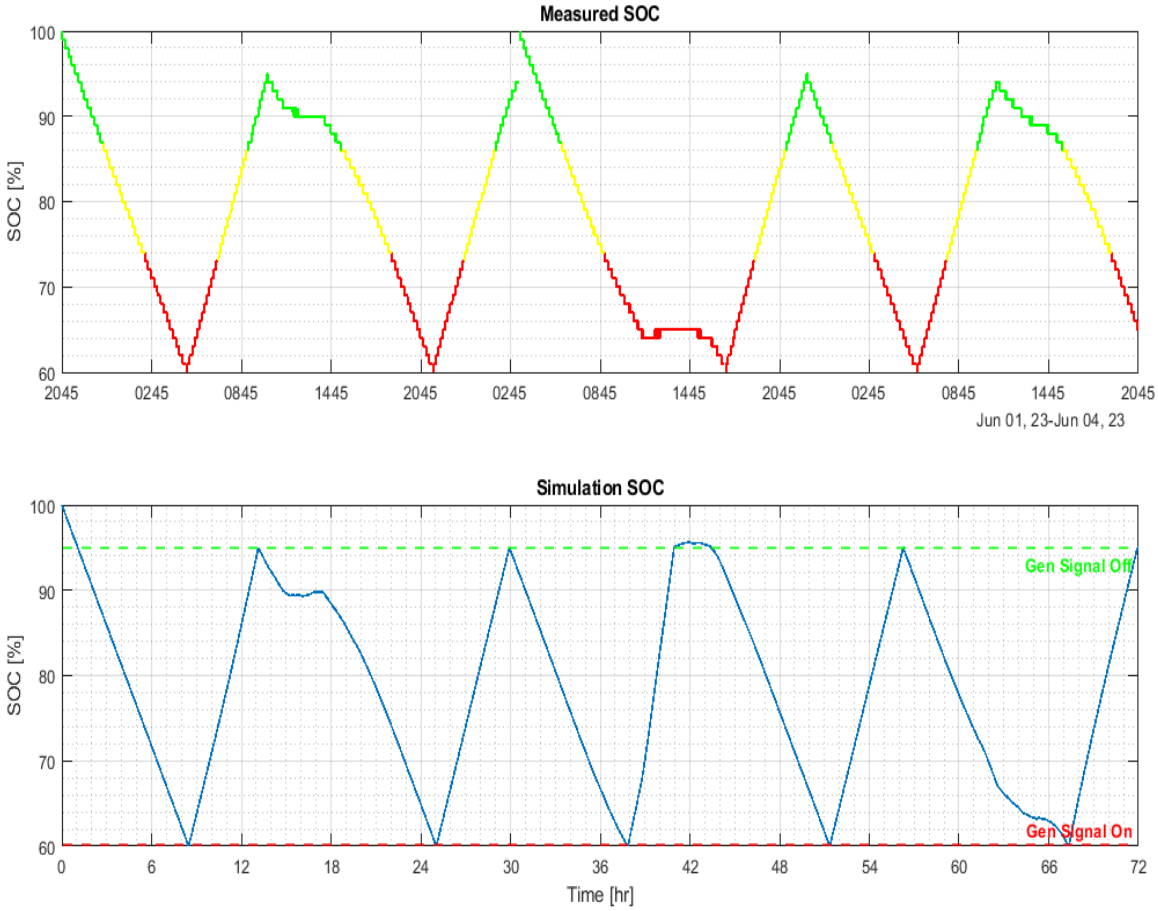

Figure 4.8. Experimental vs. Simulation SOC Comparison 1

Simulation with NREL-derived PV Profile Input

Where the comparison above used the measured PV profile from the experiment as the input to the simulation, the results presented in this section use the data derived from historical NREL data as shown in Section 3.2.4. This PV profile is derived from irradiance data for the month of June in 2022. The profile is calculated by averaging the irradiance for each day of the month and by calculating power output using the specifications of the PV panels used in the NPS microgrid (Section 4.2.1). This method is also used for the second experimental-simulation comparison.

Using this derived PV power profile produced the waveforms at the bottom of Figure 4.9. The first major discrepancy to note between the experimental the simulated measurements

is the increased power produced by the PV array in the simulations. It contributes so much power that the solar charge controller curtails the PV power output to prevent overcharging the BESS. Consequently, the generator active time for the simulation is much shorter than the generator run time in the experimental trial.

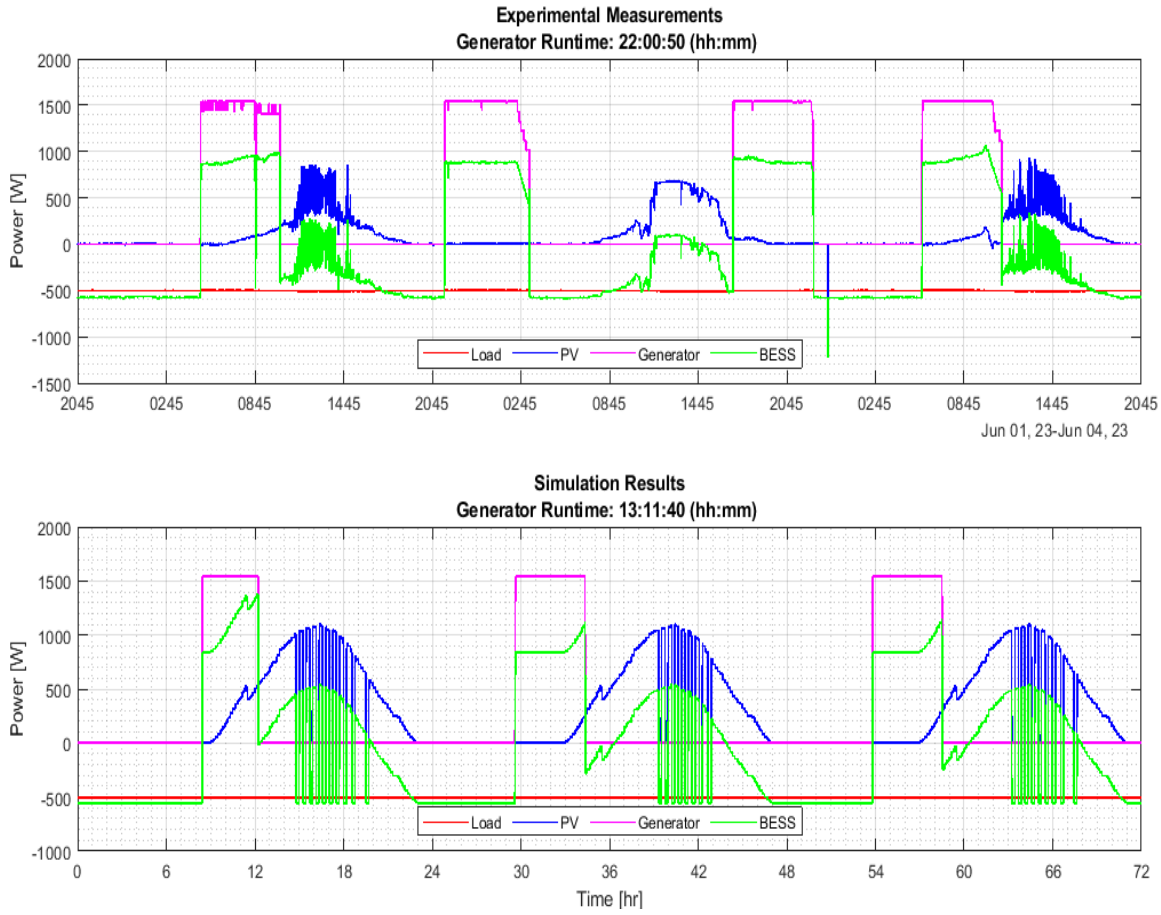

Figure 4.9. Experimental vs. Simulation Power Comparison 2

As expected, the greater PV contribution in this comparison results in the BESS reaching a full charge signaling the solar charger to regulate the power passing through it. Figure 4.10 shows the SOC in the simulation results reach 100% quickly and remain above 95% until nighttime hours.

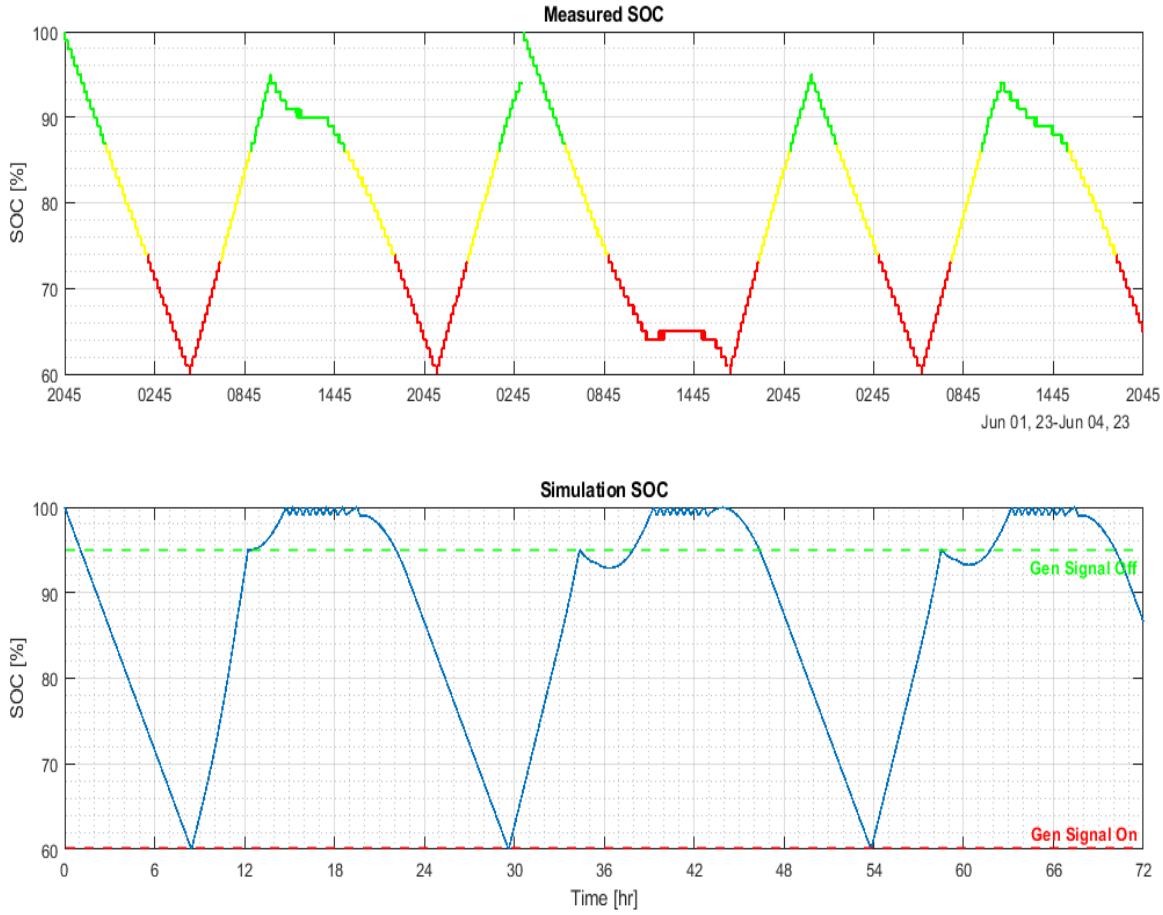

Figure 4.10. Experimental vs. Simulation SOC Comparison 2

4.3.2 Second Experimental Trial

The second experimental trial was also performed for three days, however the load was varied from 1 kW to 500 W and vice-versa at twelve hours intervals as shown in the measured plot of Figure 4.11.

Simulation with Experimental PV Profile Input

Alike the previous experiment for the first comparison, the measured PV power contribution is used as the simulation input to match most closely the environmental conditions when the experiment was conducted.

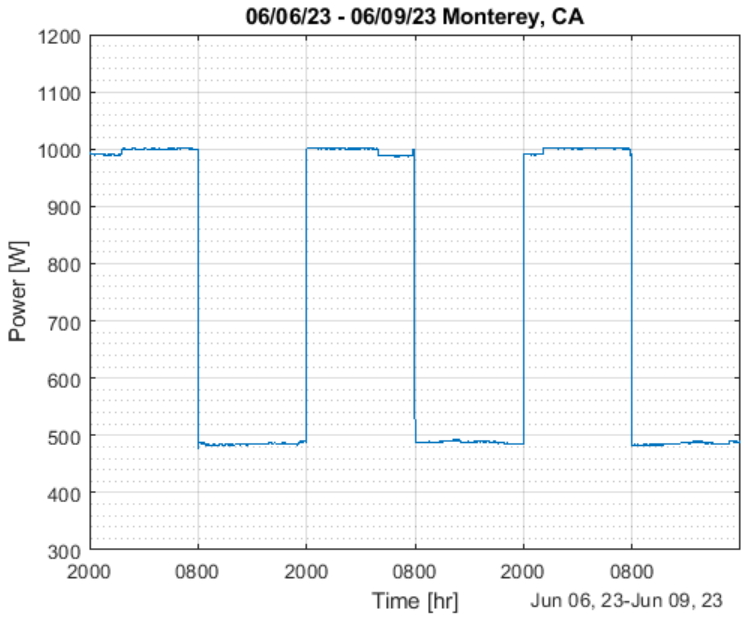

Figure 4.11. Power Drawn by the Load in the Second Experimental Trial

This difference in load power caused greater differences between the simulation and the experimental measurements. The total time the generator was active in the simulation was about one and a half hours longer than the experimental time—12% more than measured.

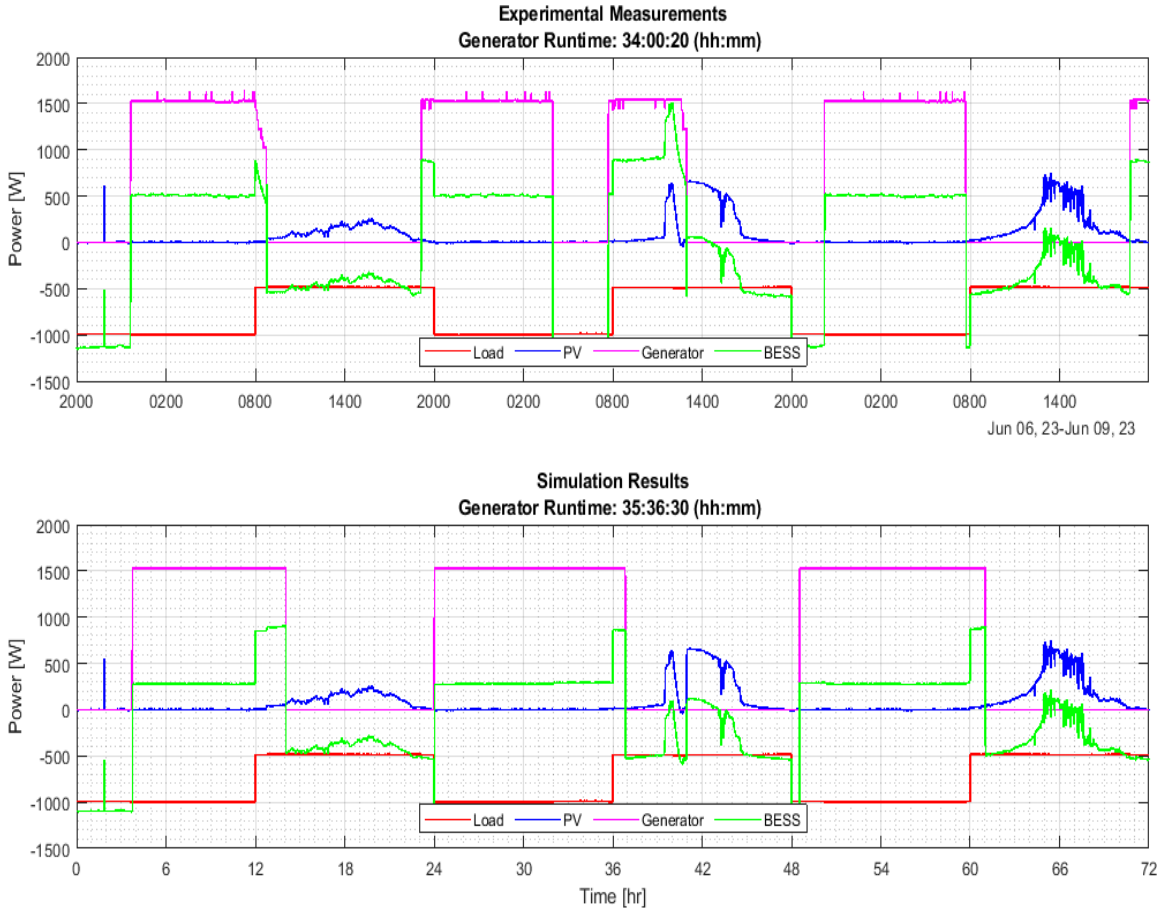

Figure 4.12. Experimental vs. Simulation Power Comparison 3

In terms of SOC, the trend in charging and discharging of the BESS did not match up as closely as expected. Notably, in Figure 4.13, the measured SOC increased linearly between 4–12h, whereas in the simulation the generator remained active longer resulting in two different charging rates during that period. The MATE3s reset the SOC to 100% on two separate occasion causing further mismatch between the simulation and experiment.

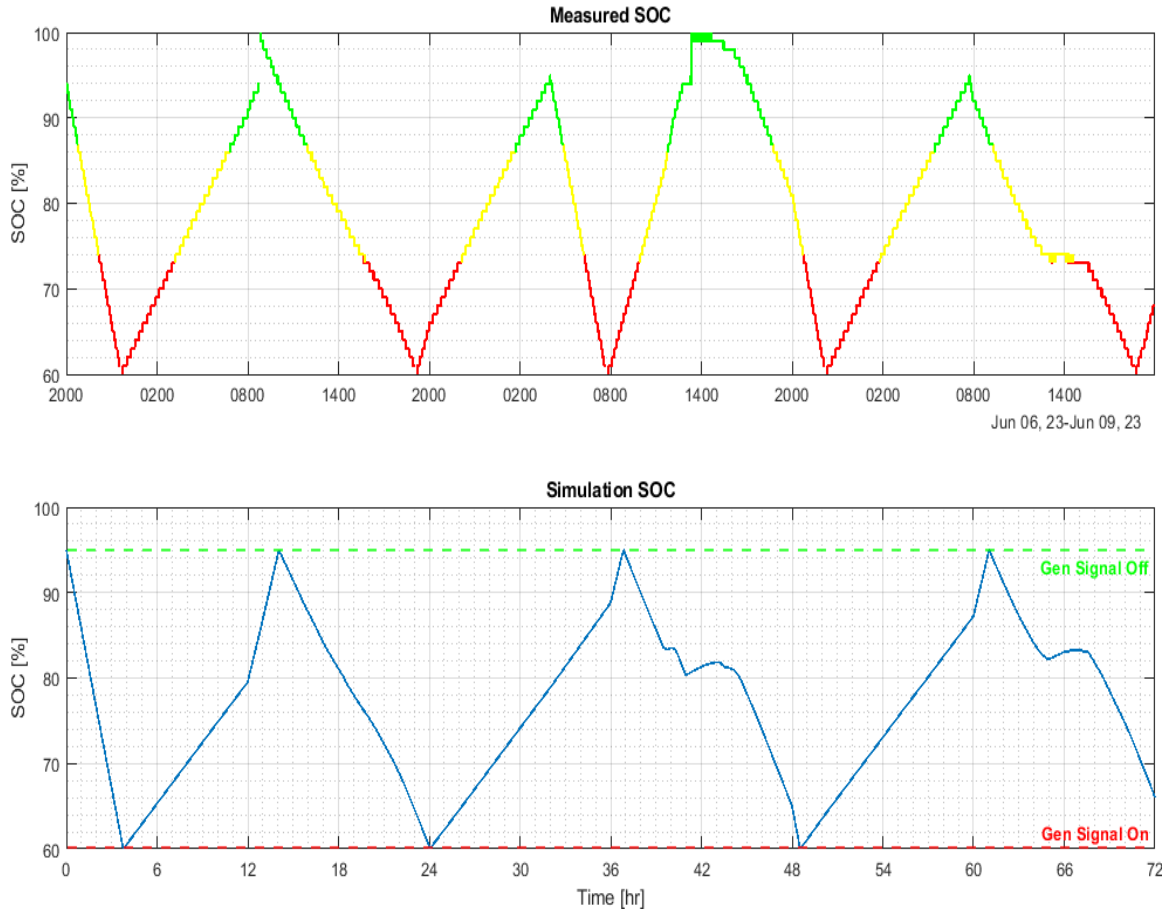

Figure 4.13. Experimental vs. Simulation SOC Comparison 3

Simulation with NREL-derived PV Profile Input

The second experimental trial comparison to the simulation now used the PV profile derived from the averaged historical data from NREL. The simulation results indicate a higher PV power contribution to the microgrid and a lower generator run time consequently. The simulation calculated the generator run time about four hours less than the experimental measurement. Figure 4.14 depicts that during the day time period the PV array contributes enough power to supply the load that it is curtailed to prevent overcharging the BESS.

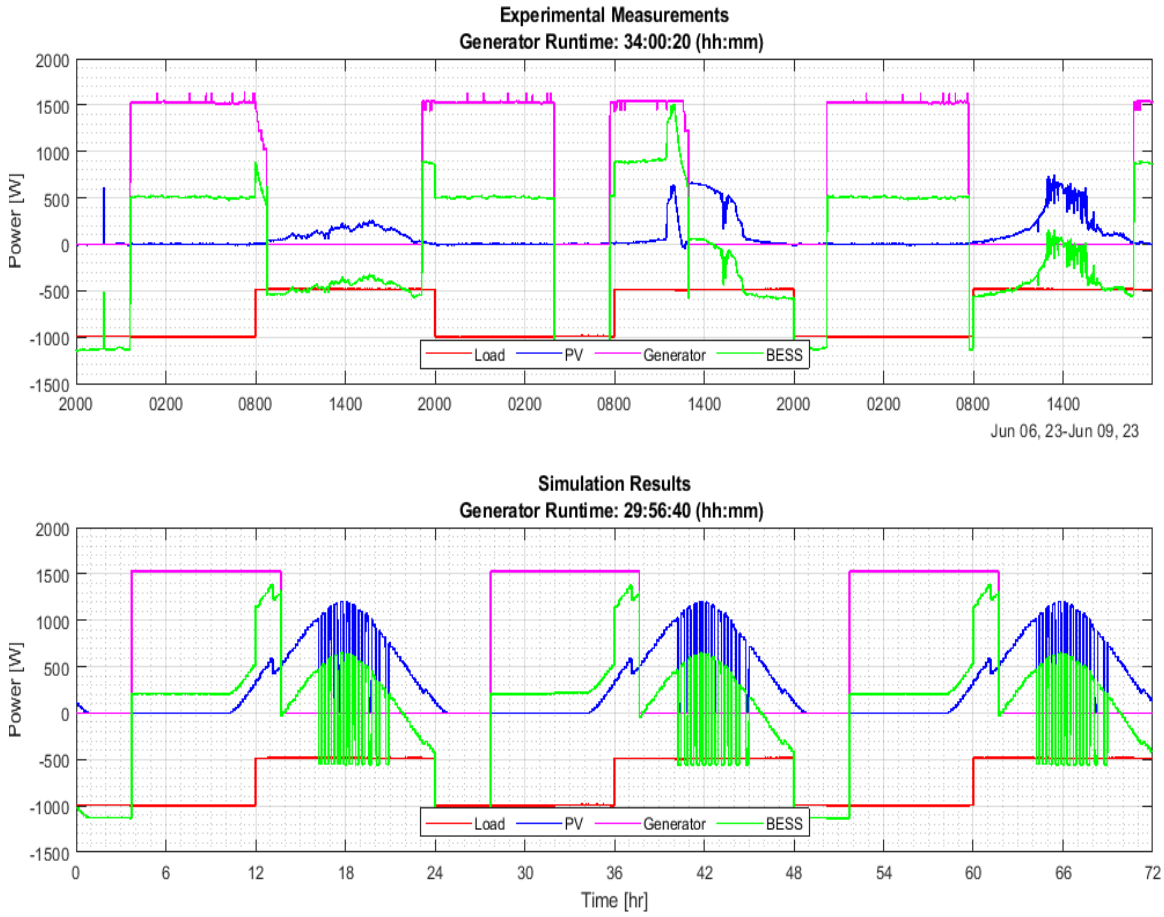

Figure 4.14. Experimental vs. Simulation Power Comparison 4

Figure 4.15 shows how SOC reaches 100% during the day period and drains faster during the night when the load is higher. The steep rates of charging when the PV array begins contributing (hour 12, 36, and 60) are not observed in the measured trial because the measured PV power contribution is not as high as in the PV contribution from the averaged historical data.

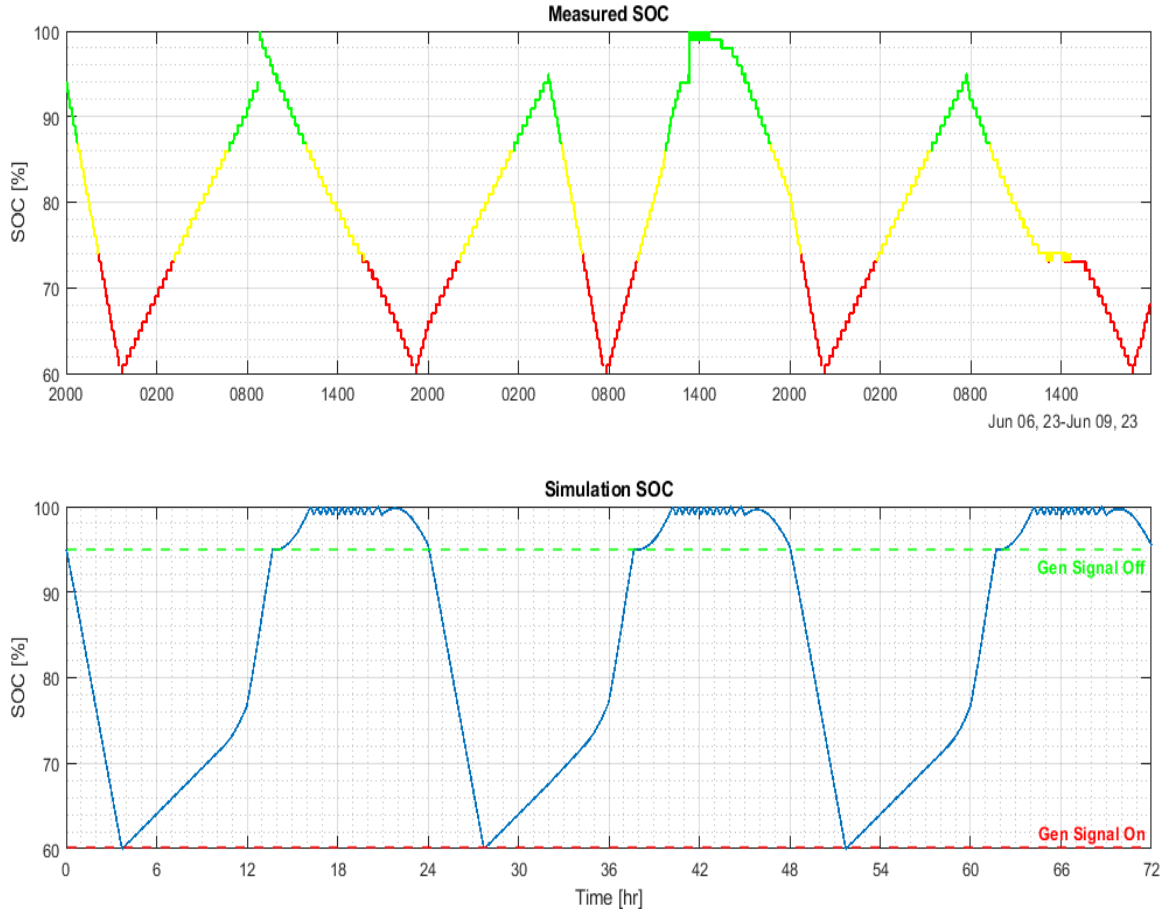

Figure 4.15. Experimental vs. Simulation SOC Comparison 4

4.4 Observations

Having completed the comparison of the experimental trials to the simulation outputs resulted in various observations of the methodology used to obtain both. The goal of these observations is to provide guidance for future improvements of the physics-based model to improve its accuracy in predicting the functionality of a microgrid.

The first observation centers on the modeling of the BESS. The method used in this simulation was a direct integration of current over time, therefore there is a linear proportionality between current and the SOC calculation. A more accurate model would include the specific charging characteristics of a battery since every battery will be different. Although the

overall trend in SOC did match the experimental measurements, implementing a charging profile specific to a certain battery would enhance the accuracy of the simulation.

For both comparisons, initially the measured power from the charge controller to the BESS was used as the PV power input to the simulation. Although it was the PV contribution for those days to get the best match between experimental measurements and simulation results, it does not account that the charge controller curtailed input power from the PV array. Figure 4.16 is a focused view of Figure 4.12 highlighting the power contribution from the measured solar charger curtailing as the BESS reaches the end of its charging cycle. The simulation uses the same PV power profile but would not be reaching the end of a charging cycle creating further inaccuracy.

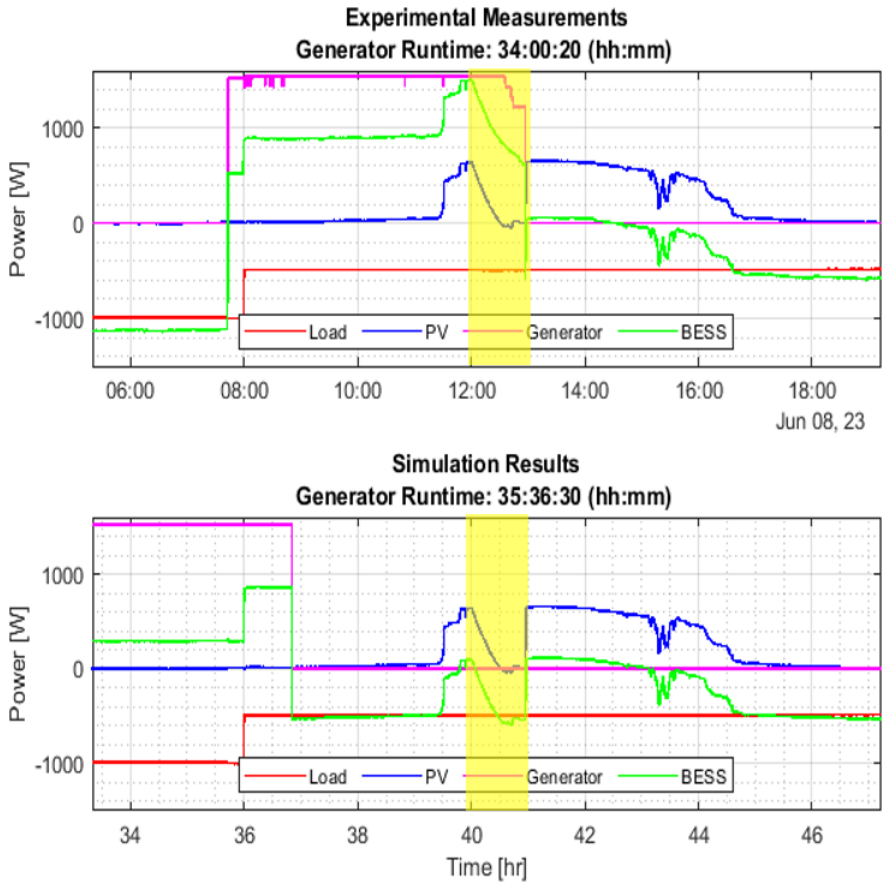

Figure 4.16. PV Power Curtailment in Experimental Measurements

The comparisons using the PV power input derived from historical NREL irradiance data was slightly less accurate. The irradiance data was the average of all the days in the month of June for only one year. Averaging over multiple years would further refine the expected output for the simulation. Another source of mismatch in PV power contribution was the configuration of the experimental setup. During the period when the experimental trials were conducted, the NPS microgrid was positioned beside a large building that obstructed direct sunlight until almost noon everyday. Figure 4.17 is a photograph taken at 10:30 AM showing the shading that causes the reduced PV power output.

Figure 4.17. PV Array Shading

The effect of shading was further observed after operating the microgrid with minimal load and no generator support for all of July 2023. Figure 4.18 shows a snapshot of two days of that month. Every day until approximately the same time the power output of the solar charger is minimized until the shading from the adjacent building had passed. This shading was also a source of mismatch between the experimental measurements and the simulation results with PV power inputs derived from NREL data.

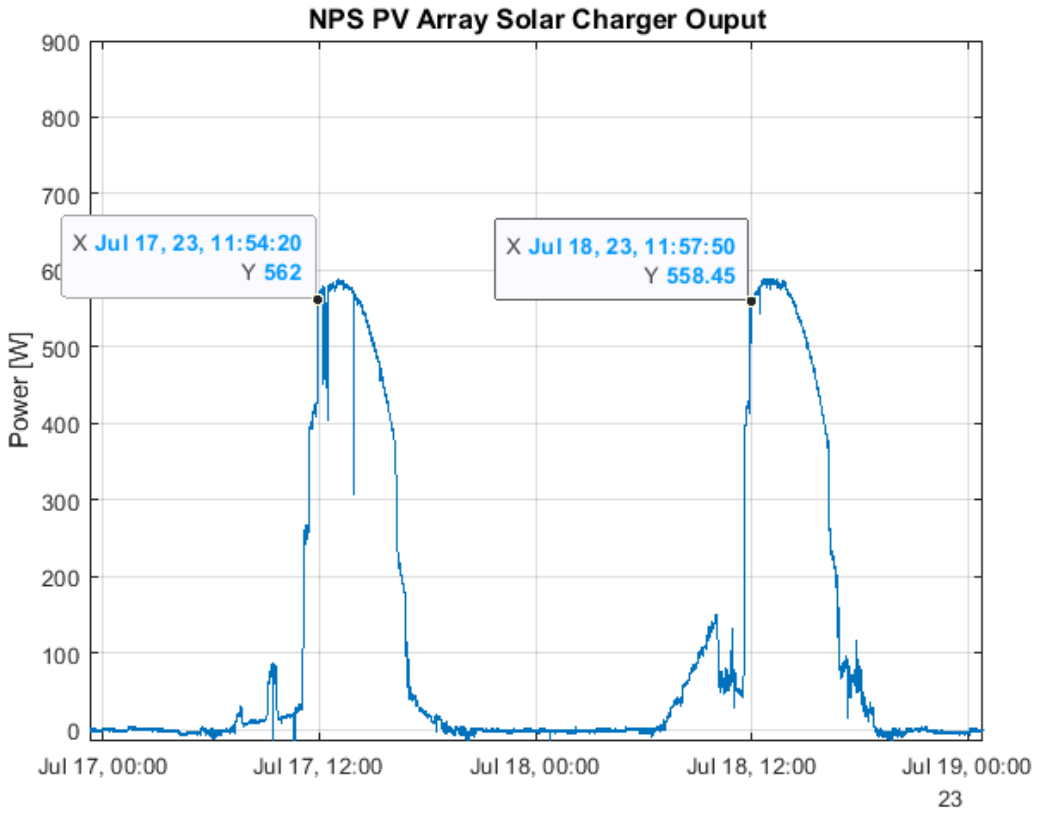

Figure 4.18. PV Shading Trend

Overall, the comparison between experimental and simulation results showed promising similarities in trends. Further refinement and improved physics-based models of the DERs will yield more realistic simulated results that can be used to design future microgrids for the DOD.

THIS PAGE INTENTIONALLY LEFT BLANK

CHAPTER 5:
Conclusion and Future Work

5.1 Conclusion

Understanding the need for future development and implementation of microgrid technology in the DOD, the research for this thesis led to the development of a physics-based model of a microgrid system based on experimental observations. The functionality of the simulation allows the user to observe the effect on performance by incorporating different configurations of a microgrid depending on the load profile which the microgrid is supporting. This capability enhances the ability of the DOD to adequately size renewable energy sources to minimize reliance on the utility grid and fossil fuel generators.

The experimental work described in Chapter 4 added significant value to the results of the simulation. Modifying the generator to automatically engage based on signals from the EMS allowed this study to better observe a microgrid operating autonomously. Additionally, incorporating the power analyzer to log measurements of power drawn by the load coupled with the adjustable electronic load enhanced the accuracy of load profiles input to the simulation. A cornerstone to visualizing the performance of a microgrid in this thesis is the data processing done in MATLAB to plot the power contributions of each component. This processing is made possible by the data-logging capability of the COTS equipment used.

The value of an accurate simulation presents itself in the design of future microgrids. With the simulation, a designer can present the performance before building the microgrid and use the results to perform cost analysis of investing more in renewable energy and energy storage equipment. The access to such results allows a designer to better inform the DOD to make decisions to best support its operations.

The simulated and experimental results presented in this thesis present a valuable step in the right direction to further implementation of microgrids in the DOD. The observations discussed in Section 4.4 identify limitations that can be overcome in future research. Having identified some of the gaps in this thesis opens the door to ideas for future work in microgrid modeling, simulation, and design.

5.2 Future Work

Throughout the research for this thesis several topics have been identified for recommended future research. Further development of the performance analysis of microgrids will provide more accurate simulation replication for microgrid design. These recommendations are identified below.

5.2.1 Irradiance Data Development

The method described in Section 3.2.4 can be further refined to provide a more accurate estimation of power to be harnessed by a PV array. The uncertainty of weather patterns will always limit the ability to predict future irradiance values. Nevertheless, researching a method to derive a PV power input to a microgrid simulation based on years of historical irradiance data coupled with historical weather data would be a valuable field to explore.

5.2.2 Modeling and Simulation Development

The physics-based model and simulations described in this research are limited by several simplifying assumptions; therefore, they do not capture the detailed functionality of the physical microgrid. To further develop this simulation, incorporating a more complex methodology for modeling a battery charging profile would better replicate experimental performance. Including a more realistic physics-based model for a battery would also open the door for simulating the control measures of an EMS. This thesis focused on controlling the microgrid based on SOC values. An EMS will control a microgrid based on much more than SOC of the BESS, including load power, battery voltage, and schedule.

Another way to expand on the simulation would be to incorporate other energy sources. Wind power can be implemented with specific parameters for a wind turbine coupled with historical and forecasted wind data for specific geographic locations. Wind power is only one of several other energy sources that could be incorporated. Including more energy sources in the physics-based model would make it a more versatile tool for microgrid designers.

APPENDIX: Generator Modification

This appendix describes the method used to incorporate the Firman generator into the NPS microgrid system. The Outback hardware used has the capability of starting the generator via a 12-V signal. The challenge of using this signal to start and stop the generator is that the Firman generator does not have automatic start capability. To overcome this challenge a COTS generator start control module is installed to process the signal from the EMS and step the generator through its starting and stopping sequence. Figure A.1 is the wiring schematic for connecting the Atkinson Electronics GSCM-Mini-60Hz to the Firman generator [24]. The generator start control module is connected to the generator as directed by the manufacturer specifications.

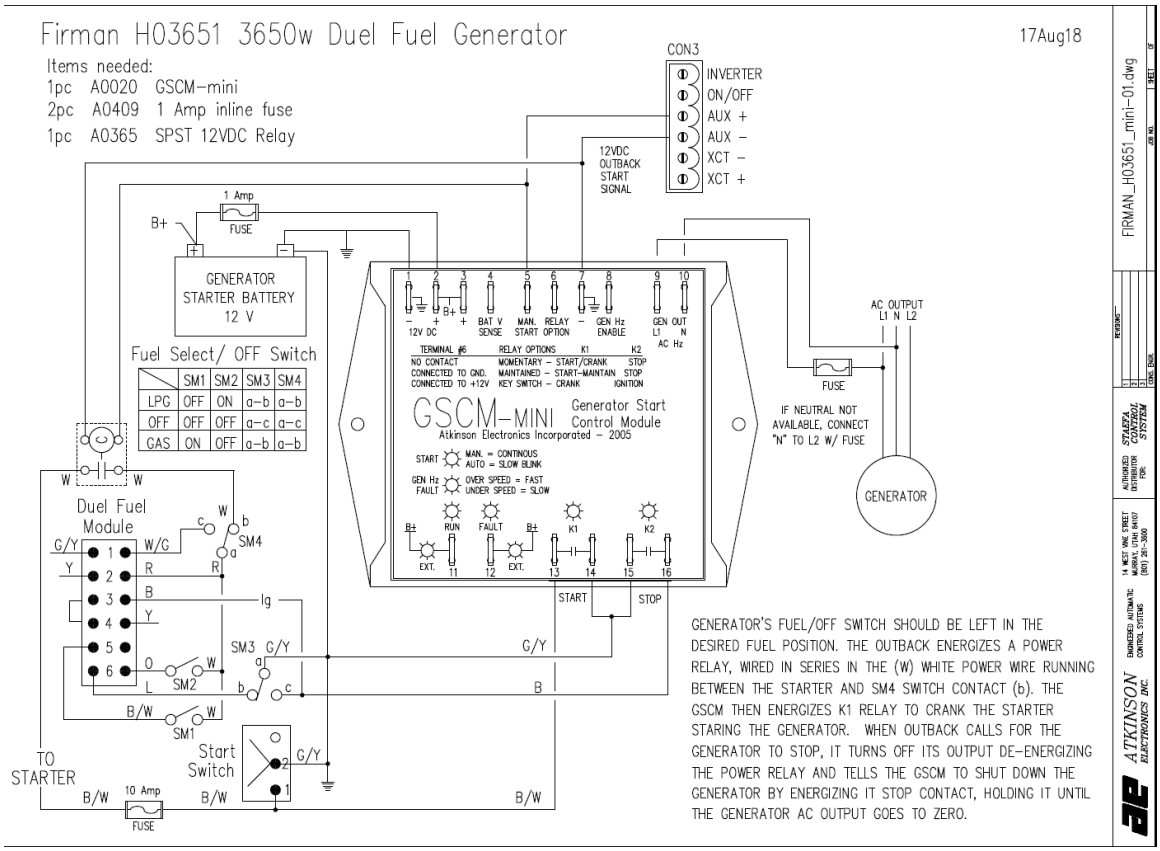

Figure A.1. Schematic of GSCM Mini. Source: [24].

Although the Firman generator does have an electric starter, it does not have an automatic carburetor choke to adjust the fuel-to-air ratio when starting which is intended to be operated manually. This manual operation is counter to the concept of the microgrid autonomously therefore modification needs to be made. Installing an electronic servo controlled by an Arduino board is the method used in this thesis. The Arduino Uno R3 in Figure A.2 manufactured by Arduino is programmed to control the servo in Figure A.3 manufactured by ANNIMOS [25], [26].

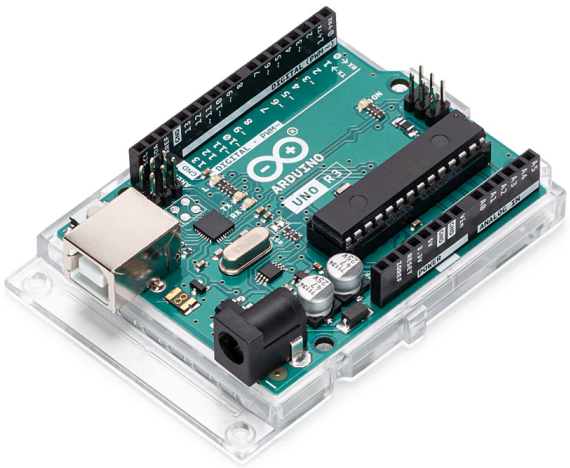

Figure A.2. Arduino Uno R3. Source: [25].

Figure A.3. ANNIMOS Servo. Source: [26].

The logic in the programming of the Arduino Uno R3 waits for the generator start control module to provide current to the starter then actuates the servo controlling the choke until the engine starts. The logic for this programming is shown in Figure A.4.

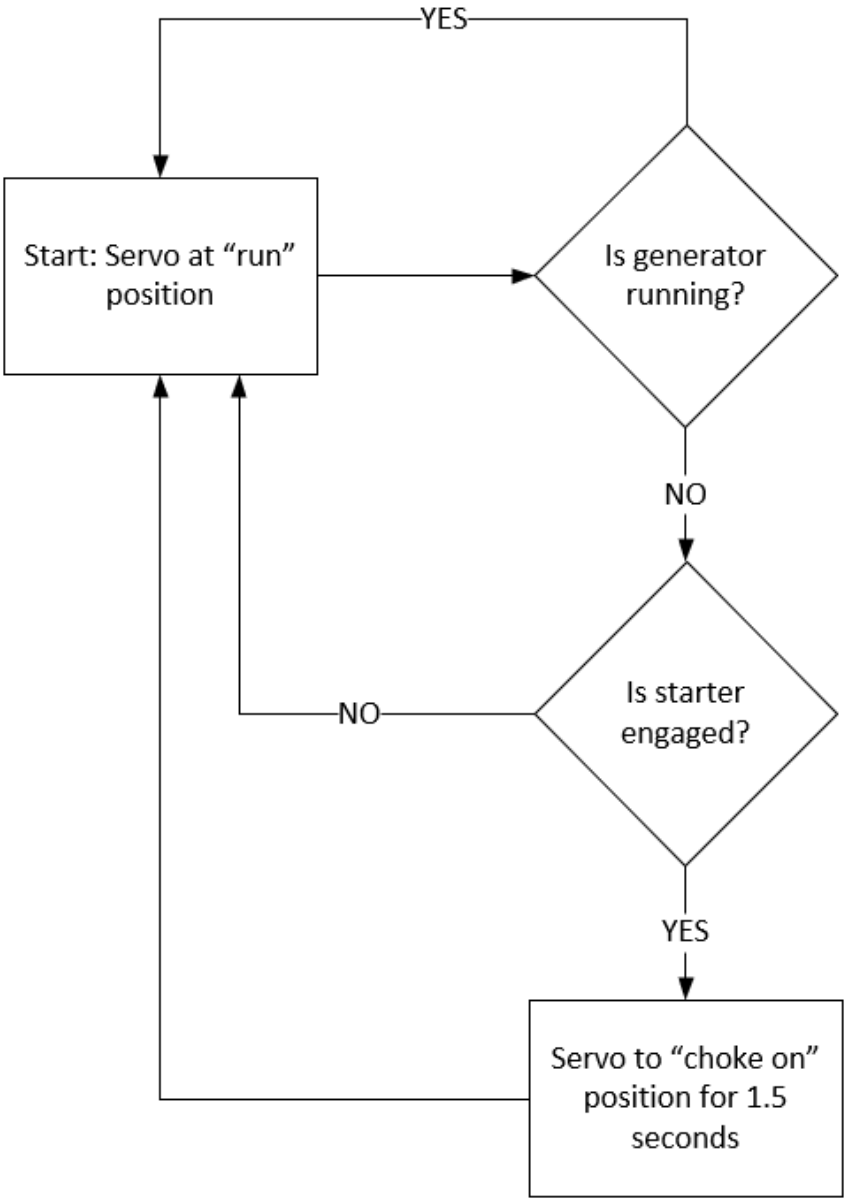

Figure A.4. Arduino Logic Controlling Servo

THIS PAGE INTENTIONALLY LEFT BLANK

List of References

[1] S. B. A. Kashem, S. De Souza, A. Iqbal, and J. Ahmed, "Microgrid in military applications," in *2018 IEEE 12th International Conference on Compatibility, Power Electronics and Power Engineering (CPE-POWERENG 2018)*, 2018, pp. 1–5.

[2] B. Naylor, "COTS microgrid lab operational at NPS," *Surge, Energy Academic Group (EAG) News*, p. 10, May 2021.

[3] L. Cohen, "History of microgrids in the US: From Pearl Street to plug-and-play," Microgrid Knowledge, blog, Jul. 22, 2019 [Online]. Available: https://www.microgridknowledge.com/about-microgrids/article/11429549/history-of-microgrids-in-the-us-from-pearl-street-to-plug-and-play

[4] B. H. Newell, "USMC Expeditionary Energy Office Report on expeditionary energy data collection within Regional Command Southwest, Afghanistan," USMC Expeditionary Energy Office, Quantico, VA: USA, 2012 [Online]. Available: https://www.hqmc.marines.mil/Portals/160/Docs/120913%20RC%20SW%20Metering%20Report.pdf

[5] R. C. Lindstrom, "Performance characterization of a mobile microgrid," M.S. thesis, Electrical and Computer Engineering Department, NPS, Monterey, CA, USA, 2022 [Online]. Available: http://hdl.handle.net/10945/71076

[6] R. Fish, "Design and modeling of hybrid microgrids in arctic environments," M.S. Thesis, Electrical and Computer Engineering Department, NPS, Monterey, CA, USA, 2020 [Online]. Available: http://hdl.handle.net/10945/66072

[7] I. S. C. C. . (SCC21), "IEEE Standard for Interconnection and Interoperability of Distributed Energy Resources with Associated Electric Power Systems Interfaces," *IEEE Std 1547-2018 (Revision of IEEE Std 1547-2003)*, pp. 1–138, 2018.

[8] D. W. Varley, "Feasibility analysis of a mobile microgrid design to support dod energy resilience goals," M.S. thesis, Naval Postrgraduate School, Monterey, CA, USA, 2022 [Online]. Available: http://hdl.handle.net/10945/70776

[9] P. P. Vergara, J. Rey, G. Ordonez, and G. Osma-Pinto, "Considerations for the design and implementation of microgrids," in *VII Simposio Internacional sobre la Calidad de la Energia Electrica - SICEL 2013*, 11 2013, p. 2. Available: https://www.researchgate.net/publication/274079892_Considerations_for_the_Design_and_Implementation_of_Microgrids

[10] J. Hofer, B. Svetozarevic, and A. Schlueter, "Hybrid AC/DC building microgrid for solar pv and battery storage integration," in *2017 IEEE Second International Conference on DC Microgrids (ICDCM)*, 2017, pp. 188–191.

[11] X. Liu, P. Wang, and P. C. Loh, "A hybrid ac/dc microgrid and its coordination control," *IEEE Trans. Smart Grid*, vol. 2, pp. 278–286, 06 2011.

[12] *Department of the Navy Climate Action 2030*, Online, Department of the Navy, Washington, D.C.: USA, 2022. Available: https://www.navy.mil/Portals/1/Documents/Department-20of-20the-20Navy-20Climate-20Action-202030.pdf

[13] D. Vergun, "DOD demonstrates mobile microgrid technology," Jun. 30, 2021 [Online]. Available: https://www.defense.gov/News/News-Stories/Article/Article/2677877/dod-demonstrates-mobile-microgrid-technology/

[14] T. M. Inc., *MATLAB version: 9.13.0 (R2022b)*, Natick, Massachusetts, United States, 2022. Available: https://www.mathworks.com

[15] The National Renewable Energy Laboratory, "NSRDB: National Solar Radiation Database." Accessed. Jun. 22, 2023 [Online]. Available: https://nsrdb.nrel.gov/

[16] B. Marion and B. Smith, "Photovoltaic system derived data for determining the solar resource and for modeling the performance of other photovoltaic systems," *Solar Energy*, vol. 147, Mar. 2017 [Online]. Available: https://doi.org/10.1016/j.solener.2017.03.043.

[17] G. Oriti, A. L. Julian, N. Anglani, and G. D. Hernandez, "Novel hybrid energy storage control for a single phase energy management system in a remote islanded microgrid," in *2017 IEEE Energy Conversion Congress and Exposition (ECCE)*. IEEE, 2017, pp. 1552–1559.

[18] Outback Power, *FLEXmax 60/80 datasheet*, FLEXmax 80, 2022 [Online]. Available: https://www.outbackpower.com/downloads/documents/charge_controllers/flexmax_6080/fm6080_datasheet.pdf

[19] GS YUASA, *Instruction manual for valve regulated lead-acid batteries for cycle use*, SLR500-2/SLR1000-2/SLR50-12, 2022 [Online]. Available: https://gsyuasa-es.com/Downloads/SLR_InstructionManual.pdf

[20] Firman Power Equipment, *Firman owner's manual dual fuel generator, H03651*, 2017 [Online]. Available: https://cdn.shopify.com/s/files/1/0527/3350/9822/files/H03651_Operators_Manual.pdf?v=1625008406

[21] Atkinson Electronics, Inc, *Generator start control module*, GSCM-mini 60Hz, 2023 [Online]. Available: https://atkinsonelectronics.com/content/product_pdfs/GSCM-mini2060Hz.PDF

[22] Outback Power, *FXR/VFXR A-Series*, VFXR3524A, 2020 [Online]. Available: https://www.outbackpower.com/downloads/documents/inverter_chargers/fxr_vfxr_a/FXR_A_specsheet.pdf

[23] Outback Power, *MATE3s series, advanced system display and controller*, MATE3s, 2020 [Online]. Available: https://www.outbackpower.com/downloads/documents/system_management/mate3s/MATE3s_specsheet.pdf

[24] Atkinson Electronics, Inc, *Generator start control module*, GSCM-mini 60Hz, 2023 [Online]. Available: https://atkinsonelectronics.com/content/product_pdfs/All-20Hookup-20Diagrams-20Merged.pdf

[25] Arduino, "Arduino Uno Rev3," Accessed. Aug. 10, 2023 [Online]. Available: https://store.arduino.cc/products/arduino-uno-rev3

[26] ANNIMOS, "ANNIMOS DS-Model Servo," Accessed. Aug. 10, 2023 [Online]. Available: https://m.media-amazon.com/images/I/81A7ByLKqDL.pdf

THIS PAGE INTENTIONALLY LEFT BLANK

Initial Distribution List

1. Defense Technical Information Center
   Ft. Belvoir, Virginia

2. Dudley Knox Library
   Naval Postgraduate School
   Monterey, California